

DOI: 10.1002/adma.((please add manuscript number))

Article type: Communication**Porous Organic Cage Thin Films and Molecular-Sieving Membranes***Qilei Song, Shan Jiang, Tom Hasell, Ming Liu, Shijing Sun, Anthony K. Cheetham, Easan Sivaniah*, and Andrew I. Cooper**

Dr. Q. Song, Prof. E. Sivaniah
Cavendish Laboratory, Department of Physics, University of Cambridge
Cambridge CB3 0HE, UK

[*] Dr. S. Jiang, Dr. T. Hasell, Dr. M. Liu, Prof. A.I. Cooper
Department of Chemistry and Centre for Materials Discovery, University of Liverpool
Liverpool L69 7ZD, UK
E-mail: aicooper@liverpool.ac.uk

S. Sun, Prof. A.K. Cheetham
Department of Materials Science and Metallurgy, University of Cambridge
Cambridge CB3 0FS, UK

[*] Prof. E. Sivaniah
Institute for Integrated Cell-Material Sciences (iCeMS), Kyoto University
Kyoto 606-8501, Japan
Email: esivaniah@icems.kyoto-u.ac.jp

Dr. Q. Song
Department of Chemical Engineering, Imperial College London
London SW7 2AZ, UK

Keywords: Porous Organic Cages, Molecular crystals, Solution-Processing, Thin films, Separation Membranes

Introduction

Microporous materials, such as conventional zeolites and activated carbons, are important in a wide range of applications including catalysis, gas storage, energy storage, and molecular separations. In recent years, organic microporous materials with well-defined structure have attracted significant attention, such as metal-organic frameworks (MOFs) or porous coordination polymers (PCPs)^[1] and covalent organic frameworks (COFs).^[2] These extended three-dimensional networks exhibit well-defined pore structures, chemical diversity, and in some cases ultrahigh surface areas. There is also increasing interest in the design and synthesis of porous molecular materials: that is, discrete organic molecules and

macromolecules where intermolecular forces are dominated by noncovalent interactions in the solid state.^[3] Porous molecular materials have some potential advantages with respect to porous extended networks: for example, they can be dissolved in common organic solvents. This enhances their solution processability, allowing them to be cast or combined with other porous materials as composites.^[4] Likewise, due to the lack of covalent bonding in porous molecular assemblies, porous molecules can exhibit structural mobility, which allows cooperative interactions between the host and guests.^[5] As an extreme case, it is also possible to prepare ‘porous liquids’ by dissolving porous cages at high concentrations in a solvent that is size-excluded from the cage cavity.^[6]

Porous materials have been extensively studied in the bulk, solid state for adsorption and separation processes. Compared to adsorption-based separation processes, membrane separation technology can often be more energy-efficient for molecular-level separations of gases and organic chemicals. In a broad context, fabrication of soluble, molecular microporous materials to functional thin films would also allow a wider range of applications beyond membranes, such as sensing, energy storage, and optoelectronics^[7]. However, the fabrication of crystalline molecular solids to thin films with well-defined structure is a challenging task. Significant progress has been made with the delicate fabrication of MOFs into thin films or membranes using techniques such as secondary crystal growth,^[8] *in situ* synthesis within a support^[9], solution-stacking of MOF nanosheets^[10], and polymer-MOF composites by coordination-driven *in situ* self-assembly^[11] or incorporation into a polymer matrix^[12].

By contrast, industrial membranes are dominated by polymers that are fabricated by simple one-step solution-processing techniques. Porous organic polymers and molecules that combine microporosity and solution processability are hence highly desirable to fabricate the next-generation porous membranes. Notable examples are polymers of intrinsic microporosity (PIMs)^[13], a new class of polymers with unique rigid and contorted macromolecular structure

and interconnected free volume that behaves like micropores (dimensions < 2 nm, according to the definition of IUPAC). In particular, some linear PIMs can be solution-processed to thin films and selective membranes for molecular separations.^[14] Further modifications of PIMs have generated membranes with remarkable performance in terms of both high permeability and high selectivity.^[15]

Discrete porous organic molecules, such as porous organic cages (POCs),^[3, 16] are another novel class of porous materials with surface areas that exceed 3000 m² g⁻¹.^[17] Recently, we prepared a series of porous organic cages (POCs) via [4+6] cycloimination reactions.^[18] As shown in Figure 1a, various types of cages can be produced by reactions between 1,3,5-triformylbenzene (TFB) with diamines, such as (1*R*,2*R*)-1,2-cyclohexanediamine (CHDA) (**CC3**), and 2-methyl-1,2-propanediamine (**CC13**). Owing to their covalent bonding and rigid shape, these molecules form internal cavities and extrinsic porosity due to inefficient packing. Pore structures and connectivity are strongly directed by the functional groups on the cage vertices such that it is possible to connect or disconnect the void volume. For example, **CC3** cage molecules tend to pack in a window-to-window arrangement to form an ordered crystalline structure (Figure 1c), leading to the three-dimensional interconnected pore network (Figure 1e). Slow crystallization of cage molecules gives a crystalline structure with long range of order, while rapid precipitation can result in short range order and defects such as crystal dislocations and grain boundaries.^[5b] Completely disordered packing of cage molecules, as visualized in Figure 1d, is also feasible by controlling the processing of cage molecules, for example by rapid removal of the solvent guest solvent molecules. For example, we used a freeze drying approach to evaporate solvents and thus to render the **CC3** in an amorphous state.^[19] The disordered packing of **CC3** cage molecules still leads to interconnected microporosity that includes both intrinsic intra-cage cavities and extrinsic inter-cage voids (Figure 1f). These amorphous cage materials showed a high level of porosity and tunable gas selectivity. The Brunauer-Emmett-Teller (BET) surface area of amorphous

CC3 reaches $898 \text{ m}^2 \text{ g}^{-1}$, which is twice the surface area of highly crystalline CC3.

Amorphous POCs can also be formed from cage molecules with different geometries and vertex groups. For example, we have demonstrated amorphous scrambled porous organic cage molecules (ASPOC), synthesized using a mixture of different diamines, which leads to a distribution of cage species that cannot pack effectively, and therefore form amorphous solids rather than crystalline materials.^[20] These molecules are also much more soluble in organic solvents, and can be used to fabricate ‘porous liquids’,^[6] or used as a stabilizer for the dispersion of metal nanoparticle catalysts in solution.^[21]

We demonstrate here the solution-processing of porous organic cage molecules into thin films, showing potential for these materials as membranes for molecular separations. To the best of our knowledge, this is the first time that POCs are fabricated into continuous and defect-free microporous thin film membranes with molecular sieving properties, without any other matrix-forming material, such as a polymer.^[4b] The unique structure of POCs and their solid-state molecular packing differentiates our work from the known literature on other membrane materials such as zeolites, polymers, MOFs, carbon molecular sieves, graphene, glass, metals, ceramics, and liquids. Hence, these results open up a new field of research on the structure and properties of porous organic cage thin films and their potential technological applications.

We fabricated thin films of POC molecules on various substrates by solution processing techniques, for example by spin coating. Spin coating is a common and established solution-processing method to coat uniform thin films from a variety of solutions on flat substrates. Compared to other solution-processing techniques, such as dip-coating and spray coating, spin-coating is the preferred method to deposit thin and uniform films on flat substrates. We start from cage molecular solids (Figure 1g) and dissolve them in organic solvents (Figure 1h), then coat these cage molecules on various substrates. The dense packed cage film coated on the glass is transparent (Figure 1i), but can be visually observed by staining with iodine,^[22]

which immediately changes the film to a yellow-brown colour upon adsorption. The spin coating process involves the equilibrium between the centrifugal forces generated at a high spinning speed and the viscous forces owing to the enhanced viscosity from solvent evaporation. In the case of small cage molecules with sizes down to 2 nm, non-covalent intermolecular forces, such as Van der Waals forces, are dominant in attracting the molecules together to form continuous films. Therefore, as visualized in Figure 1j-k, the spin-coating of cage molecules on both nonporous substrates and porous substrates leads to the formation of thin films, where the cage molecules pack in a disordered state because of the rapid solvent removal. The microporosity of cage thin films allows rapid transport and diffusion of molecules; hence, cage thin films might be used as building blocks for functional materials and devices, such as molecular sensors and separation membranes.

To demonstrate the generality and transferability of this solution-processing approach, five different types of POCs were used to prepare thin films and membranes, including a representative crystalline cage **CC3**,^[18] a related imine-cage, **CC13**,^[5b] an amorphous scrambled porous organic cage mixture (**ASPOC**) synthesized by dynamic scrambling covalent reactions,^[20] a reduced amine cage (**RCC3**),^[23] and a ‘tied’ cage (**FT-RCC3**) by reaction of amine groups in **RCC3** with carbonyls such as formaldehyde^[23] that was shown previously to have exceptional stability to water, acids, and bases. More details of synthetic chemistry are given in Figure S1 in the Supporting Information. The morphology of three representative POCs, **ASPOC**, **CC3**, and **FT-RCC3**, are shown in **Figure 2a-c**. In the solid state, **ASPOC** shows a poorly ordered morphology, while **CC3**, **CC13**, and **FT-RCC3** have a regular octahedral crystal morphology (Figure S2). X-ray diffraction (XRD) patterns of the cage solids confirmed their crystalline structure (Figure S3). FTIR spectra for cage film samples show a strong imine stretch at 1640 cm⁻¹ (Figure S4) for the imine cages.

Cage molecules were dissolved in volatile solvents, such as chloroform (boiling point, 61.15°C) or dichloromethane (39.6°C), to a predetermined concentration and purified by passing through PTFE filters (0.2 μm). In this study, the cage solution was dropped on to the substrate surface, with the liquid covering the whole surface up to the edges. The substrate was then accelerated to a very high angular velocity (~500 to 4000 rpm), resulting in a thin uniform layer coated on the surface. Continuous cage films were formed with no observable pinholes or defects, as shown in Figure 2d and 2f. Occasionally, we observed by SEM buckling and exfoliation from the substrate for **ASPOC** thin films (Figure 2e), which is likely due to stress upon fracture in liquid nitrogen. The buckling indicates that cage thin films are, to some extent, mechanically flexible. We further confirmed that similar continuous films could be fabricated from other cage molecules, including the **CC13** and **RCC3** cages (Supporting Information, Figure S5). These cage thin films are amorphous, whether they are spin-coated on silicon wafer or low-background silicon substrate, as confirmed by XRD (Figure 2m and Figure S6).

The structure of cage thin films can be easily tuned by controlling the speed of spinning and the concentration of cage molecules in solution. For example, by varying the weight concentration of **ASPOC** molecules in chloroform from 1 wt% to 5 wt%, we were able to change the thickness of the spin-cast film from 100 nm to nearly a micron (Figure S7). The porosity of cage films can be tuned from microporous to hierarchically porous by changing the composition of cage solutions, for example, use of co-solvents of dichloromethane (DCM) and methanol at different fractions. For example, **CC3** cage molecules were dissolved in a mixture of DCM and methanol, with the weight percentage of methanol in the mixture varying from 2 wt% to 40 wt%. In this case, the addition of a small amount of methanol into the solvent significantly enhanced the solubility of the **CC3**. The resulting spin-coated **CC3** films show a significantly different morphology. As shown in Figure 2(f-g) and Figure S8,

cage films spin-coated from co-solvent with low fraction of methanol (2-10wt%) are densely packed and essentially microporous with no observable mesopores or macropores. By contrast, cage solutions containing excess methanol (> 10 wt%) generate hierarchically porous films with interconnected nanoparticles with sizes at ~100 nm (Figure 2g), owing to the phase separation induced by solvent evaporation. XRD patterns confirmed that both dense and porous films are amorphous (Figure S8). Similar phase separation phenomenon occurred for **RCC3** cages and consequently macropores were formed in the films when the cage molecules were spin-coated at low speed (1000 rpm) (Figure S9).

For the more rigid, tied cage, **FT-RCC3**, hierarchically porous thin films can also be formed. As the solubility of **FT-RCC3** in chloroform or DCM was very low, a small amount of methanol was again added to the solvent to enhance the solubility of cage molecules (up to 4 wt%) so that thicker films could be prepared, but hierarchically porous films were then obtained (Figure 2h and Figure S10). In this case, the weak peaks in the XRD pattern indicate the presence of small nanocrystals. These hierarchically porous cage thin films may be useful in a range of applications, such as templates for nanostructured films, or supports for catalysis. These high-quality cage thin films have potential for absorption-based sensing based on optics or absorption spectroscopy.^[4a] Cage molecules were spin-coated on thin quartz glass substrates to form thin films with a thickness of 100 nm. Subsequently, the cage thin films were exposed to iodine solids in a glass vial. Some of the sublimed iodine was absorbed in the cage thin films, as evidenced by a dark brown coloration in this film (Fig. 1i). We tracked the UV-visible absorbance as a function of adsorption time. As shown in the Supporting Information (Figure S11), the UV-vis spectra showed a strong absorbance peak at 400 nm upon exposure to iodine. The increase of absorbance corresponds to the amount of iodine molecules adsorbed in the cage films. The UV irradiation may induce halogenation reactions of iodine with POC molecules, and hence desorption of the iodine molecules is relatively slow

and not complete even after 24 h, indicating that it is possible to utilize similar reaction strategy to modify the cage thin films.

We further fabricated POC thin film composite (TFC) membranes by spin coating cage molecules on porous anodized aluminum oxide (AAO) filter discs. The films in this work were spin-coated directly on the membrane supports without any intermediate coating or sacrificial layer. The size of cage molecules are so small that they can potentially penetrate through the surface layer of AAO support (pore size of 20 nm) and enter into the larger nanochannels (pore size of 200 nm) (Figure 2i). Pinhole and defects lead to low selectivity (close to Knudsen diffusion selectivity) and a significant increase of permeance if a continuous film is not formed. Nevertheless, defect-free films could be prepared by simply spin coating cage solutions on the surface of the AAO substrates, as shown in Figure 2j and 2k, and Supporting information Figure S12. Some cage molecules seem to be embedded in the 20 nm nano-channels in the AAO support, but they do form a continuous and defect-free skin layer. We performed XRD analyses of these thin films and confirmed that they are amorphous (Figure S13). The success rate of fabricating defect-free films was significantly enhanced by using more concentrated cage solutions (up to 4 wt%) (Figure 2l). Such higher concentration increases the viscosity of the cage solution and consequently results in thicker films while the penetration of the cage solution into the interior of the support was also limited during the spinning process. In some cases, it is relatively difficult to determine the accurate thickness for the thin film composite membranes because of the penetration into the large channels in the alumina support that occurred for some cage molecules, including **ASPOC**, **CC13**, and **RCC3**. Interestingly, the degree of penetration of cage molecules into the substrates seems to be related to the structural flexibility of the cage molecules. For the most flexible **RCC3** cages, the material cannot form a continuous film at the surface (Figure S14). In contrast, the more rigid **FT-RCC3** cages showed phase separation behaviour, as also

observed on nonporous substrates (Supporting information Figure S14). In addition, polymer thin films were also prepared from a low-free-volume polyimide (Matrimid[®] 5218) and a microporous PIM-1 polymer (SEM images are given in Figure S15), as good control for measurements of gas transport properties.

Gas transport in glassy polymeric materials follows the solution-diffusion model, where the gas molecules are absorbed in the free volume elements and diffuse through the membrane. In the case of microporous cage thin films, gas transport can also be described by the solution-diffusion model. To have a better understanding of the gas solubility and diffusivity and their relationships with the structure, we measured gas sorption properties of cage solids using various techniques. As shown in **Figure 3a**, N₂ sorption isotherms of **ASPOC** and amorphous **CC3** confirmed the presence of microporosity in these disordered solids. We also measured gas sorption isotherms at room temperature (Figure 3b) and derived the gas solubility at 1 bar (Figure 3c). Detailed isotherms are given in Figure S16. The gas solubility follows the sequence of CO₂ > CH₄ > N₂ > H₂, corresponding well to the critical temperature of gas molecules. These values of gas solubility in cage molecules are comparable to those in PIM-1 polymer.^[15b] Particularly, the high CO₂ sorption capacity in cage solids reflects the favorable solubility in micropores or free volume elements and intermolecular interactions between CO₂ gas molecules and cages.^[18b]

We further demonstrated that cage thin film composite membranes show remarkable molecular sieving performance in terms of high permeance and molecular selectivity. Single gas transport properties of cage thin films were measured at 295 K with industrially important gas molecules with different kinetic diameters, including He (2.65 Å), H₂ (2.89 Å), CO₂ (3.3 Å), Ar (3.40 Å), O₂ (3.46 Å), N₂ (3.64 Å) and CH₄ (3.82 Å),^[24] using a time-lag apparatus.^[25] First, we proved the high gas permeance through the AAO support alone (Figure S17), for example, H₂ and CO₂ permeance are 1.7×10^{-4} mol m⁻² s⁻¹ Pa⁻¹ and 4×10^{-5} mol m⁻² s⁻¹

Pa⁻¹, respectively. Therefore, the gas permeation resistance of the AAO support can be neglected in TFC membranes. In addition, we also measured the gas transport properties of polymer thin film membranes spin-cast from a dense polyimide (Matrimid[®] 5218) and a microporous PIM-1 polymer. For example, PIM-1 thin film gives an initial high CO₂ permeability of 2960 Barrer while Matrimid[®] 5218 gives a CO₂ permeability of about 10 Barrer. These gas transport properties are very close to those measured with thick polymer films in the same apparatus.^[25] Therefore, these polymer thin films serve as reliable controls for comparing the gas transport properties of cage thin films.

Gas permeation data for three representative cage thin films, **CC3**, **ASPOC**, and **CC13**, are shown in Figure 3d. The data reported here are the values measured at the point when the selectivity became stable. More detailed data are shown in the supporting information (Figure S18 and Table S1). For a typical **CC3** membrane spin-coated with 1 wt% cage solution in a co-solvent of DCM and methanol (methanol concentration of 2 wt%) at 2000 rpm, the gas permeances follow the order of H₂ > CO₂ > O₂ > CH₄ > N₂. The initial permeance of H₂ is as high as 1.53 × 10⁻⁶ mol m⁻² s⁻¹ Pa⁻¹, with high H₂/N₂ selectivity of 30 and a H₂/CH₄ selectivity close to 20. The initial CO₂ permeance is up to 9.2 × 10⁻⁷ mol m⁻² s⁻¹ Pa⁻¹ with CO₂/N₂ selectivity of ~19 and a CO₂/CH₄ selectivity of ~10. The measured gas permeances of **CC3** thin films are 10–20 times higher than that for reported MOF membranes (10–30 μm),^[26] or zeolite membranes (see Table S1),^[27] presumably because our cage films are much thinner (down to 50 nm). In the case of **ASPOC** films, gas permeances are relatively lower owing to penetration of the cages into the substrates, even though a concentrated solution (4 wt% in chloroform) was used. **CC13**, which has two methyl groups per vertex, shows much lower permeance, but still shows molecular sieving performance. For **ASPOC**, the ideal selectivity of CO₂/N₂ is surprisingly as high (25–30), which is in agreement with its favourable

adsorption of CO₂ (1.65 mmol g⁻¹) and high solubility selectivity of CO₂/N₂ (~6.5). Such behaviour is similar to that observed in glassy polymers, such as polyimide and PIMs.

We then calculated the gas permeability from permeance multiplied by thickness ($P=J \times L$). We quantified the average penetration depth as observed in SEM and assumed this depth to be the effective thickness of the membrane. We then estimated the apparent permeability. We further compare the gas transport properties in the upper bound plot of selectivity *versus* permeability. A typical H₂/N₂ gas pair is shown in **Figure 4**. For a representative 50-nm-thick **CC3** membrane, the initial H₂ permeability is about 226 Barrer, while **CC13** cages show H₂ permeability of 48 Barrer. Certainly, these cage thin films have relatively low permeability compared to PIM-1 polymer thin films (H₂ permeability close to 2000–3000 Barrer), but they are still much more permeable than conventional low-free-volume polymers (*e.g.*, H₂ permeability of Matrimid at about 20–30 Barrer). Similar results were found for other gas pairs as shown in Supporting Information (Figure S18). Based on the gas solubility and permeability, we derived the diffusion coefficients for various gas molecules ($D=P/S$). The gas diffusivities can be correlated with effective molecular size, as plotted in Figure 3f. For 24 h-aged **ASPOC**, H₂ diffusivity was as high as 9.5×10^{-7} cm² s⁻¹, while N₂ and CH₄ diffusivities were 1.1×10^{-8} cm² s⁻¹ and 6.1×10^{-9} cm² s⁻¹, respectively. The cage thin films show high diffusivity selectivity for gas pairs H₂/CO₂ (~20), H₂/N₂ (~87) and H₂/CH₄ (~155). Similar results were found for amorphous **CC3** thin films. These analyses confirm the molecular sieving properties of cage thin films, although their diffusion coefficients are relatively lower than those of rigid polymer networks.

Extensive studies on physical aging of glassy polymer thin films have shown that minor decreases of free volume with time result in significant loss of permeability.^[28] Here, we observed significant loss in gas permeability for all cage thin films (Supporting Information, Figures S18 and S19). Cages with different structures show varied aging behavior. As shown

in **Figure 4**, **ASPOC** cages give high H_2 permeability of 643 Barrer but with low selectivity of H_2/N_2 (5.8 initially). The permeability quickly decreased after aging for 24 h while selectivity increased for all gas pairs, *e.g.*, H_2 permeability decreased to 187 Barrer, while the H_2/N_2 selectivity unexpectedly increased to above 30. Similarly, CO_2 permeability dropped to 160 Barrer with CO_2/CH_4 selectivity increasing up to 17. Afterwards, the ideal gas selectivity maintained relatively stable but the gas permeability continued to decrease over 30 days. For thinner **CC3** (~50 nm), the ideal selectivity was relatively stable, but the permeability also decreased significantly. In the case of thicker **CC3** film (~300 nm), both permeability and selectivity showed immediate loss. These films remained amorphous even after aging for several months.

The complex aging phenomena of cage thin films are not yet fully understood. In this study, a very thin layer of cage molecules were coated on the alumina to form thin film composite (TFC) membranes, instead of free-standing cage membranes. Therefore, unlike free-standing polymer films,^[15] N_2 sorption and surface areas of cage TFC membranes before and after use were not easily measured. While the permeability in cage membranes decreased significantly (*e.g.* 10 times lower in 24 h for **ASPOC** membrane), gas sorption capacities of cage solids remained at high levels after being evacuated under vacuum for 24 h. Since permeability is a product of solubility and diffusivity, the loss of gas permeability may be attributed to decrease in diffusivity. From the materials perspective, these amorphous cage thin films are in metastable states that are kinetically trapped during the spin coating, which leads to an inhomogeneous density within the material. The lower density regions are in pseudo-equilibrium state and tend to pack more densely to minimize free volume over time. Previously, we designed a simulation methodology for generating amorphous cage models, and investigated gas diffusivities and diffusion mechanism in amorphous organic cage systems.^[29] We found that the contribution of the extrinsic (between cages) and intrinsic

(within cages) porosity to the total porosity has a significant effect on pore connectivity and gas diffusion pathway. Denser packing of cage molecules in the amorphous thin film state would result in a loss of extrinsic voids, which hinders the gas diffusion pathways (e.g. lower degree of connectivity of free volume or micropores, whether intrinsic or extrinsic) and consequently decreased the gas permeability in the aged cage thin films.

The molecular sieve membranes fabricated from porous organic cage molecules are insufficiently robust for many practical applications due to physical ageing, and limited chemical and thermal stability, for example, in CO₂ separation of steam-containing flue gas, or separation of H₂/CO₂ at high temperatures. For example, hydrolysis of the imine-linkages in cage molecules may occur upon exposure to water, acidic and basic conditions. Further work is in progress to produce more stable films, for example, transforming cage thin films to more chemically stable ones (such as **FT-RCC3**), or introducing stronger intermolecular forces into cages to form rigid and stable networks (e.g., by designing specific hydrogen bonding interactions between cages, or covalent crosslinking). On the other hand, the flexible property of cage solids and thin films may be useful in other applications, for example, controlled release of guest molecules (e.g. drug molecules), or adaptive materials.

In conclusion, we have demonstrated that porous organic cages can be solution-processed into coherent thin films with tunable structure and porosity. The thin films show potential in molecular sensing and selective molecular sieve membranes for molecular-level separations. The fabrication technique *via* spin coating is a simple, reproducible, and easily controlled process that yields uniform and defect-free thin films with excellent thickness control. Such ease of fabrication is achievable by the solution processability of POC molecules as building blocks. Our work also leads to better understandings of the factors that determine the phase-separation and microstructure in these systems, with which we could generate hierarchically porous cage thin films that may serve as platform for functional materials. We further demonstrate the proof-of-concept viability of molecular sieve membranes fabricated from

porous organic cage molecules. The solution processability of POCs allows coating and modification of various membranes to form composite membranes for separation of industrially and environmentally important gas molecules. Although these first-generation molecular cage films tend to densify over time, as reflected by loss in gas permeability under vacuum, they are chemically robust as shown by stable selectivity even after 30 days. Our work suggests a simple and generic approach that facilitates the fabrication of cage thin films and membranes, for example in applications such as functional coatings, composites, sensing, catalysis, separation membranes, and energy storage.

Experimental Section

Synthesis of Porous Organic Cages: All the cages, **CC3**, **CC13**, **ASPOC**, **RCC3**, and **FT-RCC3** were synthesized following previous work. **CC3** was synthesized from reactions between 1,3,5-triformylbenzene and (1*R*,2*R*)-1,2-cyclohexanediamine in dichloromethane at room temperature.^[18] The crystals were recovered by filtration, and washed with 95% ethanol/5% dichloromethane, and finally dried under vacuum. **CC13** was synthesized by reactions between 2-Methyl-1,2-propanediamine and 1,3,5-Triformylbenzene, followed by precipitation in petroleum ether, and further vacuum dried[5b]. Amorphous scrambled porous organic cages (**ASPOC**) were synthesized by co-reaction of 1,3,5-triformylbenzene (TFB) with a mixture of both 1,2-ethylenediamine (EDA) and (1*R*,2*R*)-1,2-cyclohexanediamine (CHDA) leads to an equilibrium distribution of products incorporating both EDA-linked and CHDA-linked vertices in a single cage molecule[20]. **RCC3** was synthesized by reducing **CC3** with NaBH₄ in a mixture of chloroform and methanol[23]. **FT-RCC3** was prepared by reacting the **RCC3** cages with paraformaldehyde in methanol at 70 °C[23]. The reaction was cooled to room temperature and the **FT-RCC3** was obtained after filtration and washing with methanol and further dried under vacuum.

Fabrication of cage thin films: The cage solids were dissolved in solvents to give cage solution with a certain concentration. In some cases, co-solvents of methanol (MeOH) and

dichloromethane (DCM) or chloroform was used with mass ratios changed. The cage solution was then purified by syringe filters (PTFE, 0.2 μm). After, cage thin films were prepared by spin coating the cage solution on different substrates. A drop of cage solution is applied on the substrate which is not spinning initially. Then the substrate is rotated at high speed (500-4000 rpm, typically at 2000 rpm) with an acceleration speed of 1500 rpm.

Characterization techniques: Scanning electron microscopy (SEM) analyses were performed using a Hitachi S5500 microscope. The films were fractured in air and coated with a 2-nm-thick layer of gold using an Emitech sputter coater. Wide angle X-ray diffraction (XRD) was performed with a Bruker D8 machine operated at 40 mA and 40 kV using Cu K α radiation with a step of 0.02° per second. Cage films for XRD analysis were prepared with various substrates, particularly cages were coated directly on low-background Si sample holders. Fourier Transform Infrared Spectra (FTIR) were collected on a Nicolet spectrometer. Cage films were coated on CaCl₂ disks and analyzed in transmission mode. Ultraviolet–visible absorption spectra were measured using a spectrometer, with an operating spectral range of 190–1000 nm.

Gas adsorption measurements: N₂ adsorption and desorption isotherms were measured at 77.3 K using Micromeritics 2020, or 2420 volumetric adsorption analyser. Powder samples were degassed offline at 110°C for 15 h under dynamic vacuum (10^{-5} bar) before analysis. Gas sorption isotherms of CO₂, CH₄, N₂, and H₂ were also measured at 295 K with pressure up to 1 bar.

Iodine absorption and sensing: The cage solution (1 wt%) were spin-coated on quartz substrate at a speed of 2000 rpm. Prior to spin coating, quartz plates were cleaned with acetone and isopropanol in ultrasound bath for 10 min, respectively. The thin films coated on quartz plates were exposed to iodine solids to allow the adsorption of iodine in the films. The UV-visible absorption spectra were tracked as a function of sorption time.

Fabrication of thin film composite membranes: POCs based thin film composite membranes were prepared by simply spin coating cage solutions on porous support. Anodized aluminum oxide (AAO) membrane (Anodisc, Whatman) with a surface layer of 20 nm nanopores were used as porous supports. The gas permeances through the support are significantly higher than those in cage thin films. The membrane disc as ordered has an annular polypropylene ring. The support membrane was fixed on a PTFE substrate for spin-coating. The inorganic membrane support is quite brittle, so care was taken to fix and transfer the support from spin-coating to gas permeation tests.

Gas permeation tests: Pure gas permeation tests were carried out at temperature of 22°C and feed pressure of 1 bar, using a constant-volume pressure-increase apparatus described in detail elsewhere^[15b, 25]. The membrane was loaded in the apparatus and thoroughly evacuated with a vacuum pump (Edwards RV3) prior to gas permeation measurements. The gas permance (J , mol m⁻² s⁻¹ Pa⁻¹) was measured directly. The ideal selectivity for a gas pair (A/B) is calculated from the ratio of their permeance. The uncertainties of the as-measured permeance at the moment of test are within ±10%, and selectivity within ±15%. Gas permeability (P) was calculated from multiplying the permance with the thickness of the effective layer of POC film ($P=J \times L$). P is expressed in Barrer (1 Barrer=10⁻¹⁰ cm³(STP)cm·cm⁻²·s⁻¹·cmHg⁻¹). The solubility of gas molecules in POCs were quantified from gas sorption measurements up to 1 bar at 295 K. The diffusion coefficient (D) (at 1 bar) is calculated from the permeability ($D=P/S$).

Supporting Information

Supporting Information is available from the Wiley Online Library or from the author.

Acknowledgements

This work was financially supported by the Engineering and Physical Sciences Research Council (EPSRC, UK, EP/H000925/1), European Research Council (ERC) and an NPRP grant from the QNRF (Qatar). Q.S. acknowledges financial support of an Imperial College Junior Research Fellowship.

Received: ((will be filled in by the editorial staff))

Revised: ((will be filled in by the editorial staff))

Published online: ((will be filled in by the editorial staff))

References

- [1] a)O. M. Yaghi, M. O'Keeffe, N. W. Ockwig, H. K. Chae, M. Eddaoudi, J. Kim, *Nature* **2003**, *423*, 705-714; b)S. Kitagawa, R. Kitaura, S.-i. Noro, *Angew. Chem., Int. Ed.* **2004**, *43*, 2334-2375.
- [2] a)H. M. El-Kaderi, J. R. Hunt, J. L. Mendoza-Cortes, A. P. Cote, R. E. Taylor, M. O'Keeffe, O. M. Yaghi, *Science* **2007**, *316*, 268-272; b)A. P. Côté, A. I. Benin, N. W. Ockwig, M. O'Keeffe, A. J. Matzger, O. M. Yaghi, *Science* **2005**, *310*, 1166-1170.
- [3] J. R. Holst, A. Trewin, A. I. Cooper, *Nat. Chem.* **2010**, *2*, 915-920.
- [4] a)M. Brutschy, M. W. Schneider, M. Mastalerz, S. R. Waldvogel, *Adv. Mater.* **2012**, *24*, 6049-6052; b)A. F. Bushell, P. M. Budd, M. P. Attfield, J. T. A. Jones, T. Hasell, A. I. Cooper, P. Bernardo, F. Bazzarelli, G. Clarizia, J. C. Jansen, *Angew. Chem., Int. Ed.* **2013**, *52*, 1253-1256; c)T. Hasell, H. Zhang, A. I. Cooper, *Adv. Mater.* **2012**, *24*, 5732-5737; d)T. Hasell, J. A. Armstrong, K. E. Jelfs, F. H. Tay, K. M. Thomas, S. G. Kazarian, A. I. Cooper, *Chem. Comm.* **2013**, *49*, 9410-9412.
- [5] a)L. Chen, P. S. Reiss, S. Y. Chong, D. Holden, K. E. Jelfs, T. Hasell, M. A. Little, A. Kewley, M. E. Briggs, A. Stephenson, K. M. Thomas, J. A. Armstrong, J. Bell, J. Busto, R. Noel, J. Liu, D. M. Strachan, P. K. Thallapally, A. I. Cooper, *Nat. Mater.* **2014**, *13*, 954-960; b)T. Hasell, J. L. Culshaw, S. Y. Chong, M. Schmidtman, M. A. Little, K. E. Jelfs, E. O. Pyzer-Knapp, H. Shepherd, D. J. Adams, G. M. Day, A. I. Cooper, *J. Am. Chem. Soc.* **2014**, *136*, 1438-1448.
- [6] N. Giri, M. G. Del Pópolo, G. Melaugh, R. L. Greenaway, K. Rätzke, T. Koschine, L. Pison, M. F. C. Gomes, A. I. Cooper, S. L. James, *Nature* **2015**, *527*, 216-220.
- [7] A. Bétard, R. A. Fischer, *Chem. Rev.* **2011**, *112*, 1055-1083.
- [8] Y. S. Li, H. Bux, A. Feldhoff, G. N. Li, W. S. Yang, J. Caro, *Adv. Mater.* **2010**, *22*, 3322-3326.
- [9] A. J. Brown, N. A. Brunelli, K. Eum, F. Rashidi, J. R. Johnson, W. J. Koros, C. W. Jones, S. Nair, *Science* **2014**, *345*, 72-75.
- [10] Y. Peng, Y. S. Li, Y. J. Ban, H. Jin, W. M. Jiao, X. L. Liu, W. S. Yang, *Science* **2014**, *346*, 1356-1359.
- [11] R. Zhang, S. Ji, N. Wang, L. Wang, G. Zhang, J.-R. Li, *Angew. Chem., Int. Ed.* **2014**, *53*, 9775-9779.
- [12] a)T. Rodenas, I. Luz, G. Prieto, B. Seoane, H. Miro, A. Corma, F. Kapteijn, F. X. Llabrés i Xamena, J. Gascon, *Nat. Mater.* **2014**, *14*, 48-55; b)L. Dobrzańska, G. O. Lloyd, C. Esterhuysen, L. J. Barbour, *Angew. Chem., Int. Ed.* **2006**, *45*, 5856-5859.
- [13] a)P. M. Budd, E. S. Elabas, B. S. Ghanem, S. Makhseed, N. B. McKeown, K. J. Msayib, C. E. Tattershall, D. Wang, *Adv. Mater.* **2004**, *16*, 456-459; b)P. M. Budd, B. S. Ghanem, S. Makhseed, N. B. McKeown, K. J. Msayib, C. E. Tattershall, *Chem. Commun.* **2004**, *10*, 230-231; c)N. B. McKeown, P. M. Budd, K. J. Msayib, B. S. Ghanem, H. J. Kingston, C. E. Tattershall, S. Makhseed, K. J. Reynolds, D. Fritsch, *Chem.-Eur. J.* **2005**, *11*, 2610-2620.
- [14] a)N. Du, H. B. Park, G. P. Robertson, M. M. Dal-Cin, T. Visser, L. Scoles, M. D. Guiver, *Nat. Mater.* **2011**, *10*, 372-375; b)M. Carta, R. Malpass-Evans, M. Croad, Y. Rogan, J. C. Jansen, P. Bernardo, F. Bazzarelli, N. B. McKeown, *Science* **2013**, *339*, 303-307.
- [15] a)Q. Song, S. Cao, P. Zavala-Rivera, L. P. Lu, W. Li, Y. Ji, S. A. Al-Muhtaseb, A. K. Cheetham, E. Sivaniah, *Nat. Commun.* **2013**, *4*, 1918; b)Q. Song, S. Cao, R. H. Pritchard, B. Ghalei, S. A. Al-Muhtaseb, E. M. Terentjev, A. K. Cheetham, E. Sivaniah, *Nat. Commun.* **2014**, *5*, 4813; c)Q. Song, S. Cao, R. H. Pritchard, H. Qiblawey, E. M. Terentjev, A. K. Cheetham, E. Sivaniah, *J. Mater. Chem. A* **2016**, *4*, 270-279.

- [16] M. Mastalerz, *Chem. Commun.* **2008**, 4756-4758.
- [17] G. Zhang, O. Presly, F. White, I. M. Oppel, M. Mastalerz, *Angew. Chem., Int. Ed.* **2014**, *53*, 1516-1520.
- [18] a) J. T. A. Jones, T. Hasell, X. Wu, J. Bacsá, K. E. Jelfs, M. Schmidtman, S. Y. Chong, D. J. Adams, A. Trewin, F. Schiffman, F. Cora, B. Slater, A. Steiner, G. M. Day, A. I. Cooper, *Nature* **2011**, *474*, 367-371; b) T. Tozawa, J. T. A. Jones, S. I. Swamy, S. Jiang, D. J. Adams, S. Shakespeare, R. Clowes, D. Bradshaw, T. Hasell, S. Y. Chong, C. Tang, S. Thompson, J. Parker, A. Trewin, J. Bacsá, A. M. Z. Slawin, A. Steiner, A. I. Cooper, *Nat. Mater.* **2009**, *8*, 973-978.
- [19] T. Hasell, S. Y. Chong, K. E. Jelfs, D. J. Adams, A. I. Cooper, *J. Am. Chem. Soc.* **2011**, *134*, 588-598.
- [20] S. Jiang, J. T. A. Jones, T. Hasell, C. E. Blythe, D. J. Adams, A. Trewin, A. I. Cooper, *Nat Commun* **2011**, *2*, 207.
- [21] J.-K. Sun, W.-W. Zhan, T. Akita, Q. Xu, *J. Am. Chem. Soc.* **2015**, *137*, 7063-7066.
- [22] T. Hasell, M. Schmidtman, A. I. Cooper, *J. Am. Chem. Soc.* **2011**, *133*, 14920-14923.
- [23] M. Liu, M. A. Little, K. E. Jelfs, J. T. A. Jones, M. Schmidtman, S. Y. Chong, T. Hasell, A. I. Cooper, *J. Am. Chem. Soc.* **2014**, *136*, 7583-7586.
- [24] L. M. Robeson, *J. Membr. Sci.* **1991**, *62*, 165-185.
- [25] Q. Song, S. K. Nataraj, M. V. Roussenova, J. C. Tan, D. J. Hughes, W. Li, P. Bourgoïn, M. A. Alam, A. K. Cheetham, S. A. Al-Muhtaseb, E. Sivaniah, *Energy Environ. Sci.* **2012**, *5*, 8359-8369.
- [26] a) H. Bux, A. Feldhoff, J. Cravillon, M. Wiebcke, Y. S. Li, J. Caro, *Chem. Mater.* **2011**, *23*, 2262-2269; b) Y. Li, F. Liang, H. Bux, W. Yang, J. Caro, *J. Membr. Sci.* **2010**, *354*, 48-54; c) A. Huang, W. Dou, J. Caro, *J. Am. Chem. Soc.* **2010**, *132*, 15562-15564; d) A. Huang, H. Bux, F. Steinbach, J. Caro, *Angew. Chem., Int. Ed.* **2010**, *49*, 4958-4961; e) H. Bux, F. Liang, Y. Li, J. Cravillon, M. Wiebcke, J. Caro, *J. Am. Chem. Soc.* **2009**, *131*, 16000-16001.
- [27] a) X. Yin, G. Zhu, Z. Wang, N. Yue, S. Qiu, *Microporous Mesoporous Mater.* **2007**, *105*, 156-162; b) J. C. Poshusta, V. A. Tuan, J. L. Falconer, R. D. Noble, *Ind. Eng. Chem. Res.* **1998**, *37*, 3924-3929; c) A. Huang, F. Liang, F. Steinbach, T. M. Gesing, J. Caro, *J. Am. Chem. Soc.* **2010**, *132*, 2140-2141.
- [28] a) J. H. Kim, W. J. Koros, D. R. Paul, *Polymer* **2006**, *47*, 3094-3103; b) K. Nagai, T. Masuda, T. Nakagawa, B. D. Freeman, I. Pinnau, *Prog. Polym. Sci.* **2001**, *26*, 721-798.
- [29] S. Jiang, K. E. Jelfs, D. Holden, T. Hasell, S. Y. Chong, M. Haranczyk, A. Trewin, A. I. Cooper, *J. Am. Chem. Soc.* **2013**, *135*, 17818-17830.
- [30] P. M. Budd, K. J. Msayib, C. E. Tattershall, B. S. Ghanem, K. J. Reynolds, N. B. McKeown, D. Fritsch, *J. Membr. Sci.* **2005**, *251*, 263-269.
- [31] a) N. Du, H. B. Park, M. M. Dal-Cin, M. D. Guiver, *Energy Environ. Sci.* **2012**, *5*, 7306-7322; b) C. G. Bezzu, M. Carta, A. Tonkins, J. C. Jansen, P. Bernardo, F. Bazzarelli, N. B. McKeown, *Adv. Mater.* **2012**, *24*, 5930-5933; c) M. Carta, M. Croad, R. Malpass-Evans, J. C. Jansen, P. Bernardo, G. Clarizia, K. Friess, M. Lanč, N. B. McKeown, *Adv. Mater.* **2014**, *26*, 3526-3531; d) B. S. Ghanem, R. Swaidan, E. Litwiller, I. Pinnau, *Adv. Mater.* **2014**, *26*, 3688-3692; e) B. S. Ghanem, N. B. McKeown, P. M. Budd, J. D. Selbie, D. Fritsch, *Adv. Mater.* **2008**, *20*, 2766-2771.
- [32] L. M. Robeson, *J. Membr. Sci.* **2008**, *320*, 390-400.

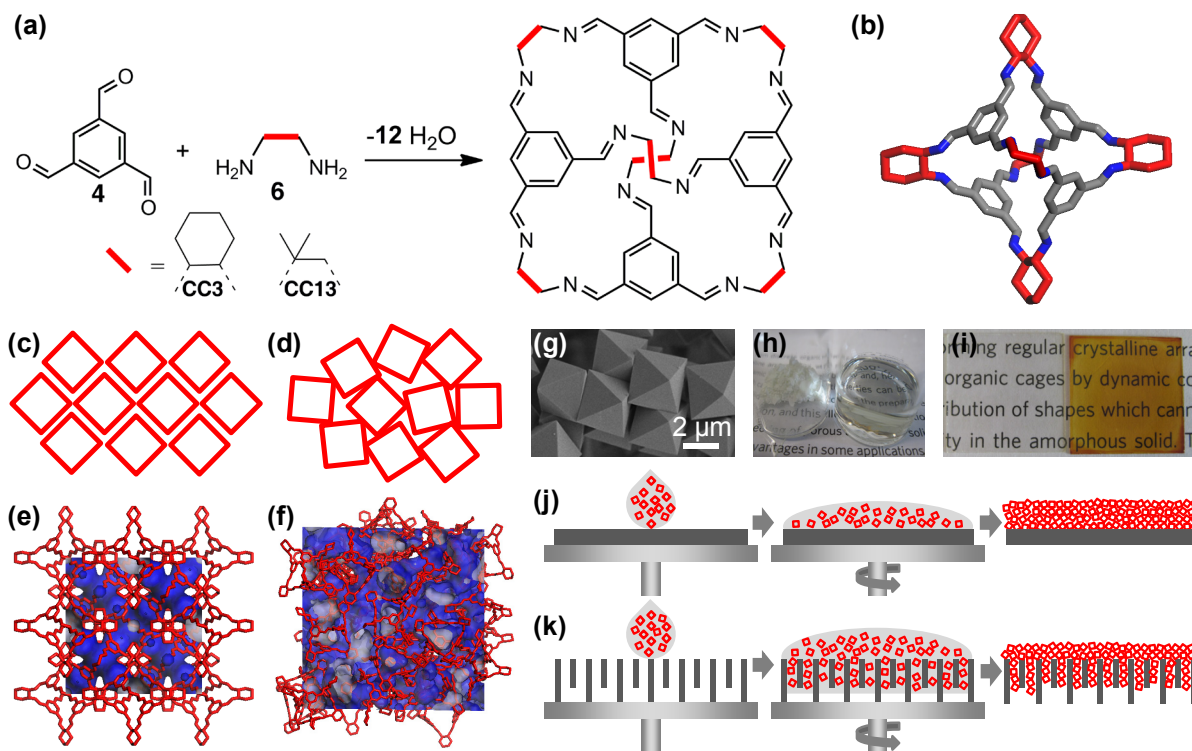


Figure 1. Synthesis of porous organic cages (POCs) and solution-processing of POCs into thin films. (a) Synthetic pathways and chemical structures of POCs. (b) 3-D crystalline structure of CC3 cage. (c) Schemes showing ordered assembly of cage molecules into crystals (each cage molecule represented by a square), and (d) disordered packing of cage molecules in the amorphous state. Molecular simulation of (e) crystalline structure and (f) amorphous packing of cage CC3, with the Connolly surface shown in blue probed by N₂ molecules (kinetic diameter of 3.64 Å). (g) SEM image of CC3 crystals, (h) Photograph of crystalline CC3 cage solids (left glass vial) and solution of cage molecules dissolved in solvent (right glass vial). (i) Photograph of cage thin films spin-coated on cover glass slides (left: transparent cage film coated on glass alone, right: cage film stained with iodine). (j-k) Scheme illustrating spin-coating of cage solution into an ultrathin layer of cage films on (j) nonporous substrate, and (k) porous substrate, forming thin film composite (TFC) membrane with molecular sieving function.

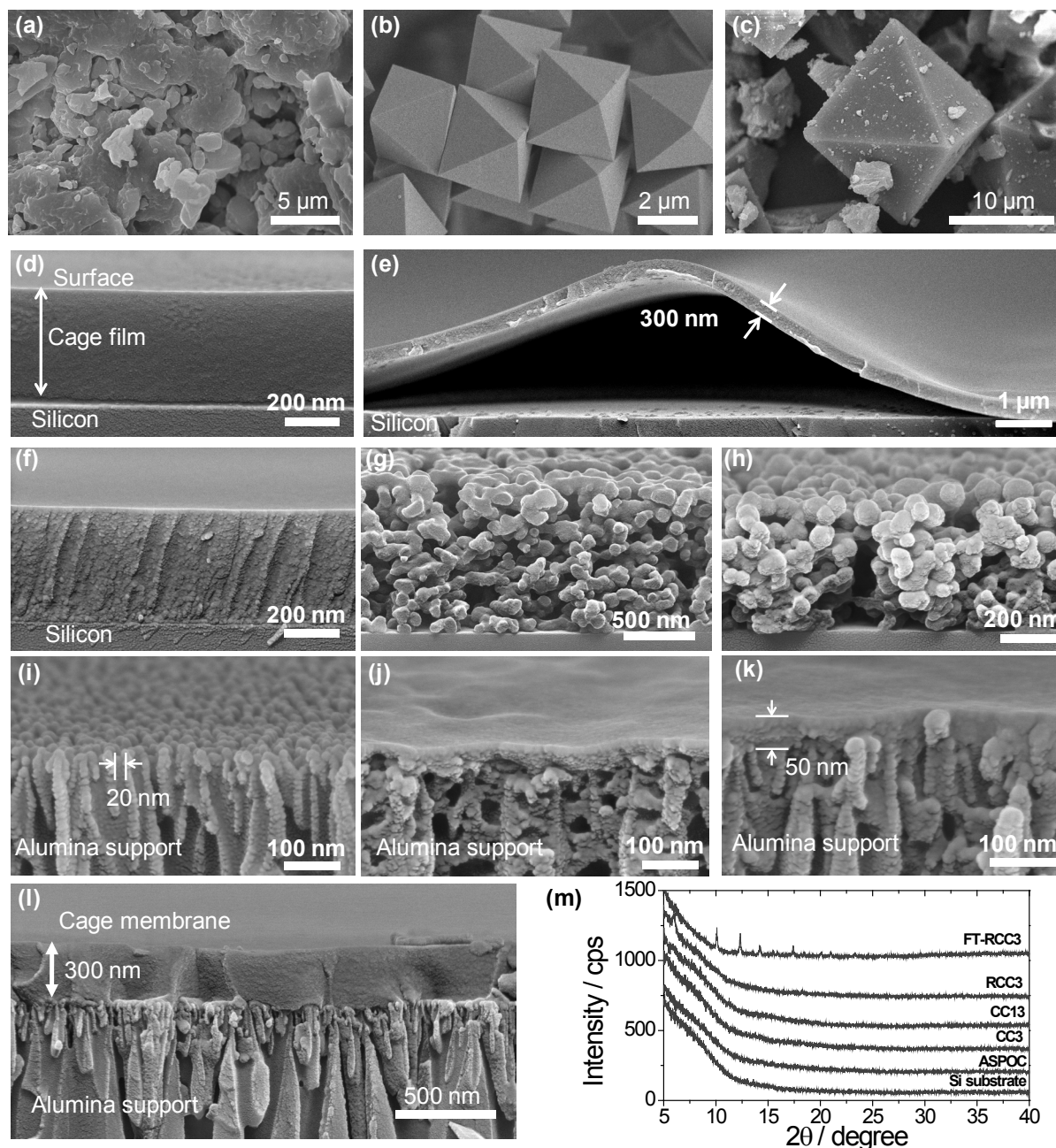


Figure 2. Morphology and structure of POC thin films coated on nonporous and porous substrates. (a) ASPOC powder. (b) CC3 crystals. (c) FT-RCC3 crystals. (d) ASPOC thin film spin-coated from ASPOC solution in chloroform (4 wt%, weight percentage of cages in solvent). (e) Buckling of ASPOC thin films occasionally occurred upon exposure to fracture in liquid nitrogen. (f) CC3 thin film, spin-coated from CC3 cage solution (4 wt%, weight percentage of cages in solvent) in a mixture of co-solvent of MeOH (2 wt%)/DCM (98 wt%). (g) CC3 film, spin-coated from CC3 cage solution (4 wt% in solvent) in a mixture of co-solvent of MeOH (15 wt%)/DCM (85 wt%). (h) FT-RCC3 film, spin-coated from FT-RCC3 cage solution (4 wt% in solvent) in a mixture of co-solvent of MeOH (2 wt%)/DCM (98 wt%). (i) Cross-sectional SEM of porous anodized aluminum oxide (AAO) support. (j) Cross-sectional SEM of ASPOC cages coated on Al₂O₃ support. ASPOC cage solution (4 wt% in chloroform) was spin-coated at 2000 rpm for 1 min. (k) Cross-sectional SEM of 50-nm thick CC3 thin film coated on Al₂O₃ support. CC3 cage solution (1 wt% in solvent) in a co-solvent of MeOH (2wt%)/DCM (98 wt%) was spin-coated at 2000 rpm for 1 min. (l) Cross-sectional SEM of 300-nm thick CC3 thin film coated on alumina support. CC3 cage solution (4 wt%) in a co-solvent of MeOH (2 wt%)/DCM (98 wt%) was spin-coated on alumina support at 2000 rpm for 1 min. (m) X-ray diffraction of POC thin films coated on low-background silicon substrates.

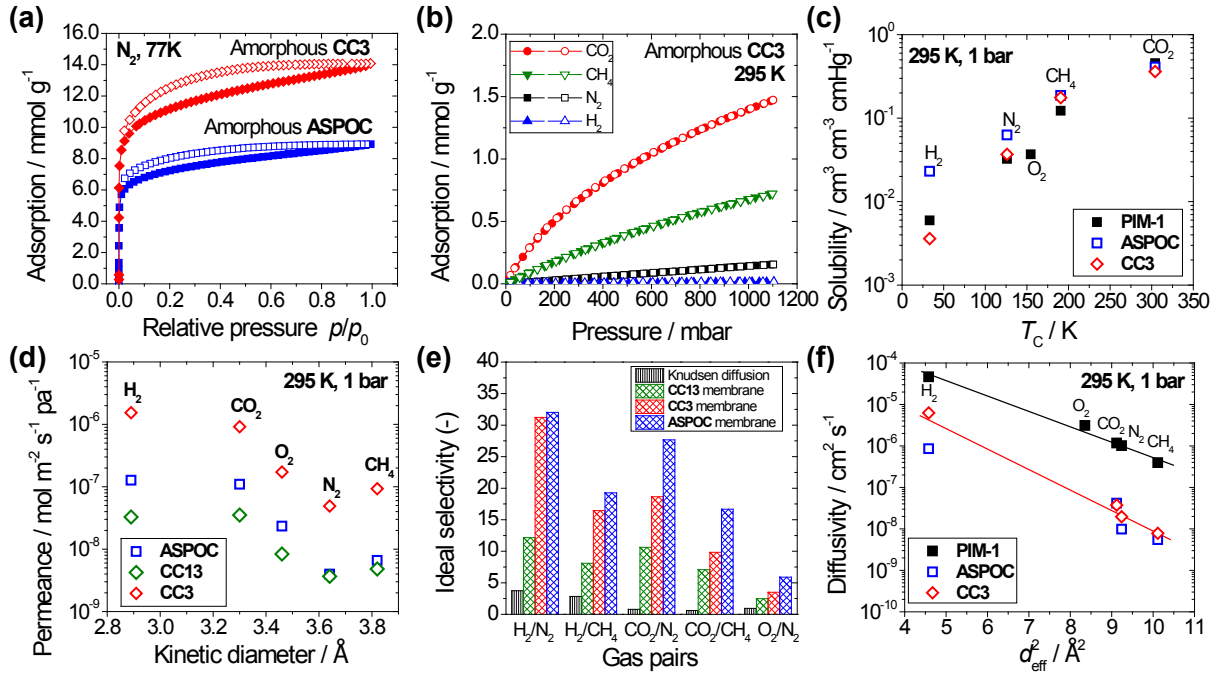


Figure 3. Gas sorption and transport properties for cage materials. (a) N_2 adsorption-desorption isotherms at 77K for ASPOC and amorphous CC3 (freeze-dried). (b) Gas sorption isotherms for amorphous CC3 at 295 K. (c) gas solubility at 295 K and 1 bar. (d) Gas permeance as a function of kinetic diameter of gas molecules through POC thin film composite membranes. Three representative POC membranes are shown here: ASPOC, CC13, and CC3 (50 nm). ASPOC membrane was aged under vacuum for 24 h, CC13 and CC3 (50 nm) membranes were as prepared. (e) Ideal gas selectivity of gas pairs derived from the ratio of permeance for corresponding gas molecules. (f) Gas diffusivity as a function of square of effective molecular diameter (d_{eff}) of gas molecules at 295 K. Lines are added to guide eyes. The solubility and diffusivity of a representative polymer of intrinsic microporosity (PIM-1) are included for comparison in (c) and (f), measured using the same method.^[15b]

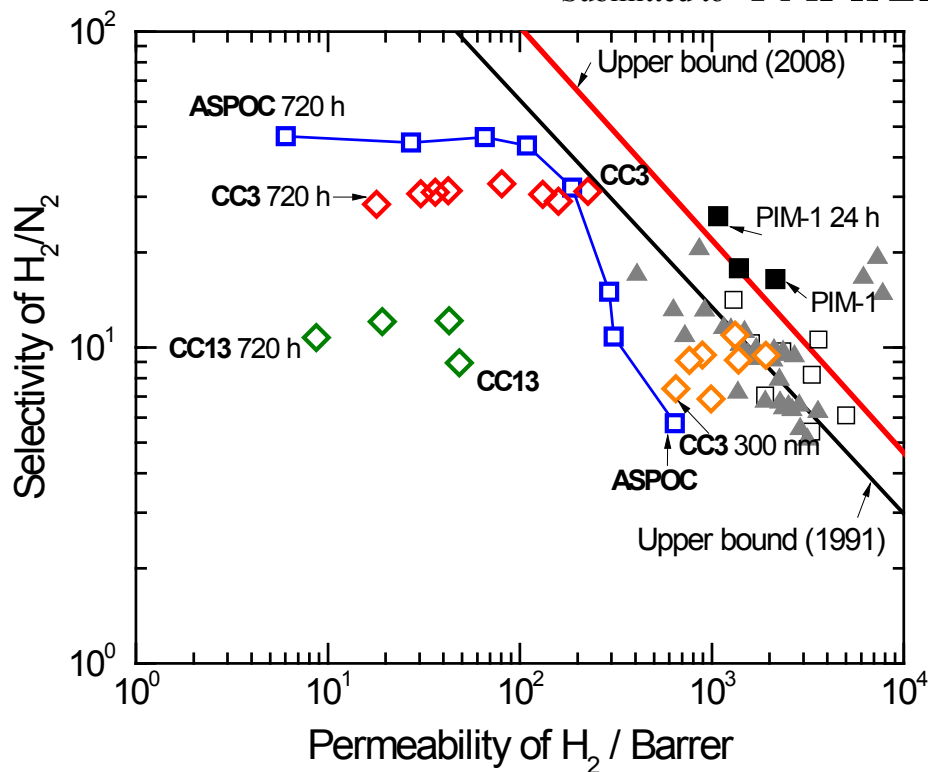


Figure 4. Upper bound plot of selectivity *versus* permeability. The change of gas transport properties of four cage thin film membranes (under vacuum) for a typical H₂/N₂ gas pair are presented, including ASPOC (aged for 30 days), CC13 (aged for 30 days), amorphous CC3 (50 nm, aged for 30 days) and another 300 nm-thick CC3 (aged for 48 h). Solid squares: PIM-1 thin film. Open squares: PIM-1 in the literature.^[13a, 30] Triangles: Other PIMs reported in the literature^[14b, 31]. Upper bounds were reported by Robeson in 1991,^[24] and 2008,^[32] respectively.

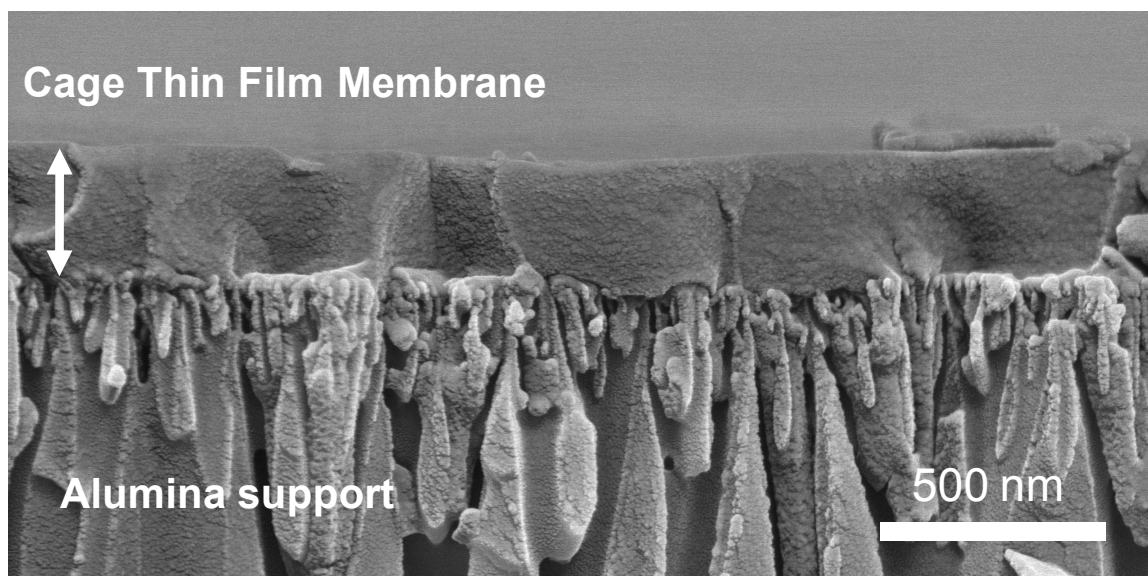
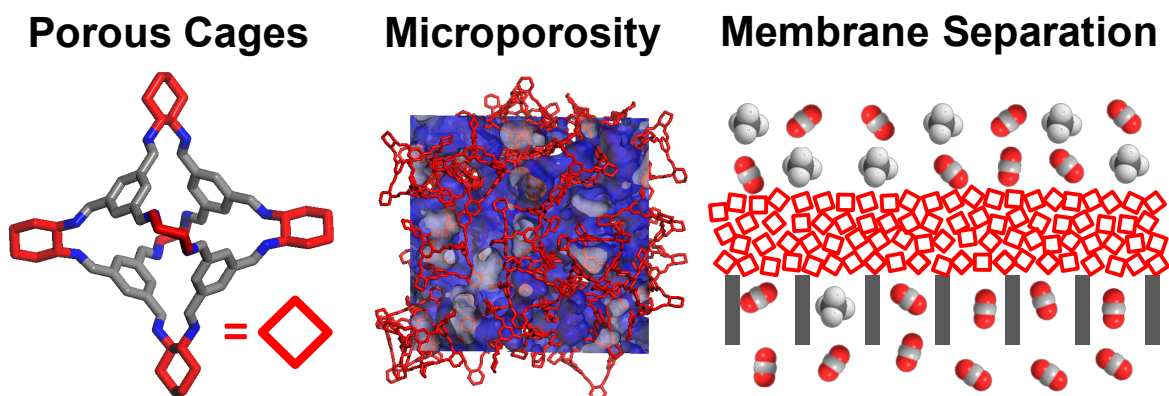
Porous organic cage molecules are fabricated to thin films and molecular-sieving membranes. Cage molecules are solution cast on various substrates to form amorphous thin films, with the structures tuned by tailoring the cage chemistry and processing conditions. For the first time, uniform and pinhole-free microporous cage thin films are formed and demonstrated as molecular-sieving membranes for selective gas separation.

Keywords: Porous Organic Cages, Solution-Processing, Molecular Crystals, Thin films, Membranes

Q. Song, S. Jiang, T. Hasell, M. Liu, S. Sun, A.K. Cheetham, E. Sivaniah*, and A. I. Cooper*

Porous Organic Cage Thin Films and Molecular-Sieving Membranes

ToC figure ((Please choose one size: 55 mm broad × 50 mm high **or** 110 mm broad × 20 mm high. Please do not use any other dimensions))



Supporting Information

Porous Organic Cage Thin Films and Molecular-Sieving Membranes

Qilei Song, Shan Jiang, Tom Hasell, Ming Liu, Shijing Sun, Anthony K. Cheetham, Easan Sivaniah*, and Andrew I. Cooper*

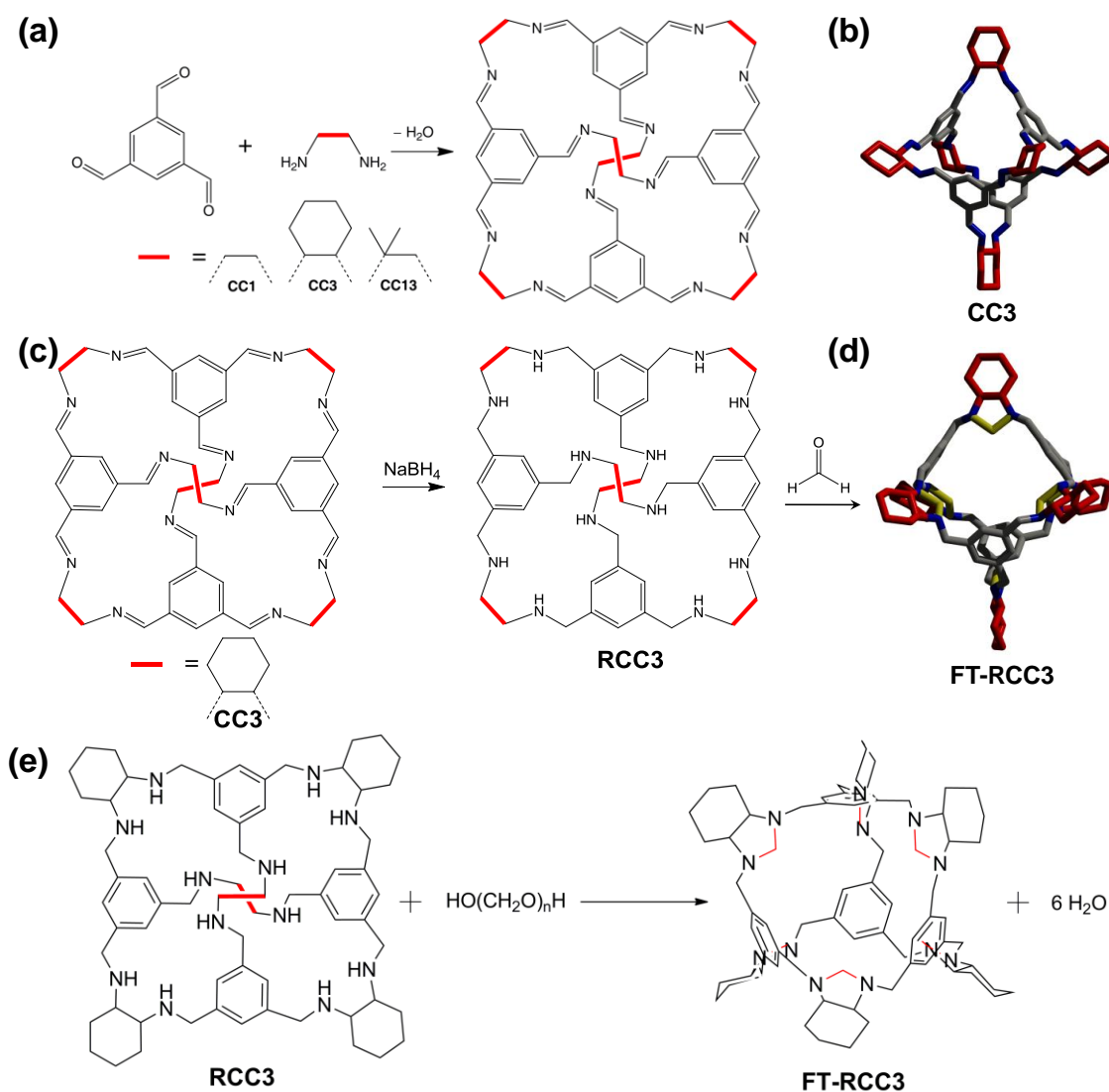


Figure S1. Synthesis and chemical structure of porous organic cages. (a) Synthesis of organic cage modules (CC1, CC3, and CC13) via a [4 + 6] cycloimination reaction. ASPOC is synthesized from co-reaction of two different diamines: 1,2-ethylenediamine (EDA) and (1*R*,2*R*)-diaminocyclohexane (CHDA) with 1,3,5-triformylbenzene (TFB). (b) 3D crystalline structure of CC3. (c) Reduction of CC3 cage to RCC3 cage by NaBH₄. Desolvated RCC3 shows a significant loss of porosity due to the collapse of its much more flexible cage cavity. RCC3 can be transformed to a more rigid and shape persistent cage, (d) 3D crystalline structure of FT-RCC3, by (e) reaction of amine groups with carbonyls such as formaldehyde (or depolymerized from paraformaldehyde by heating).^[1]

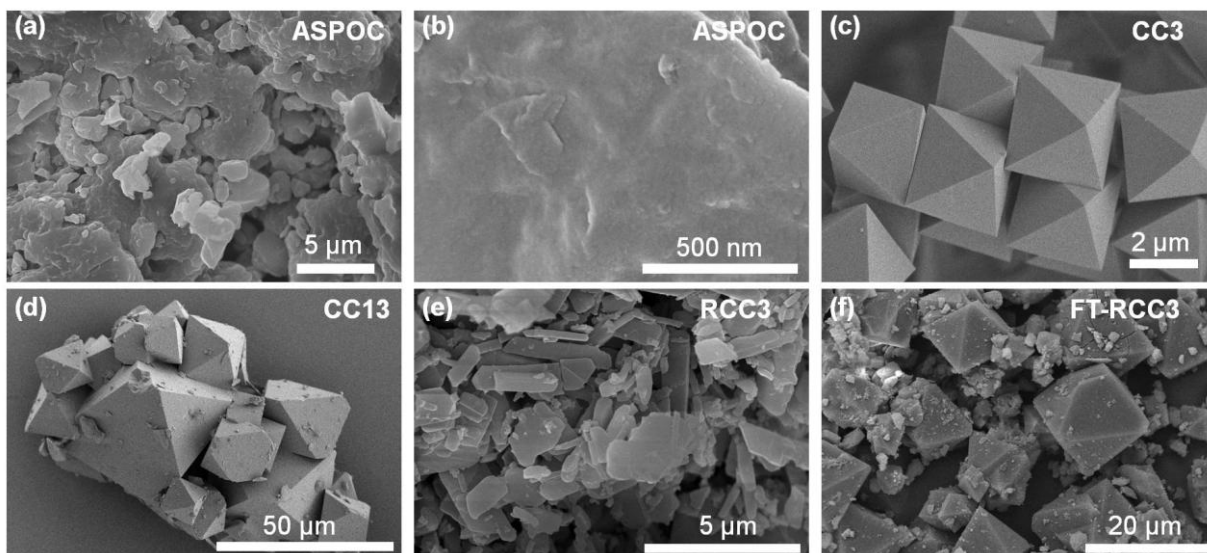


Figure S2. SEM images of POCs as prepared in the powder form. (a) ASPOC, (b) enlargement of ASPOC, (c) CC3, (d) CC13, (e) RCC3, (f) FT-RCC3.

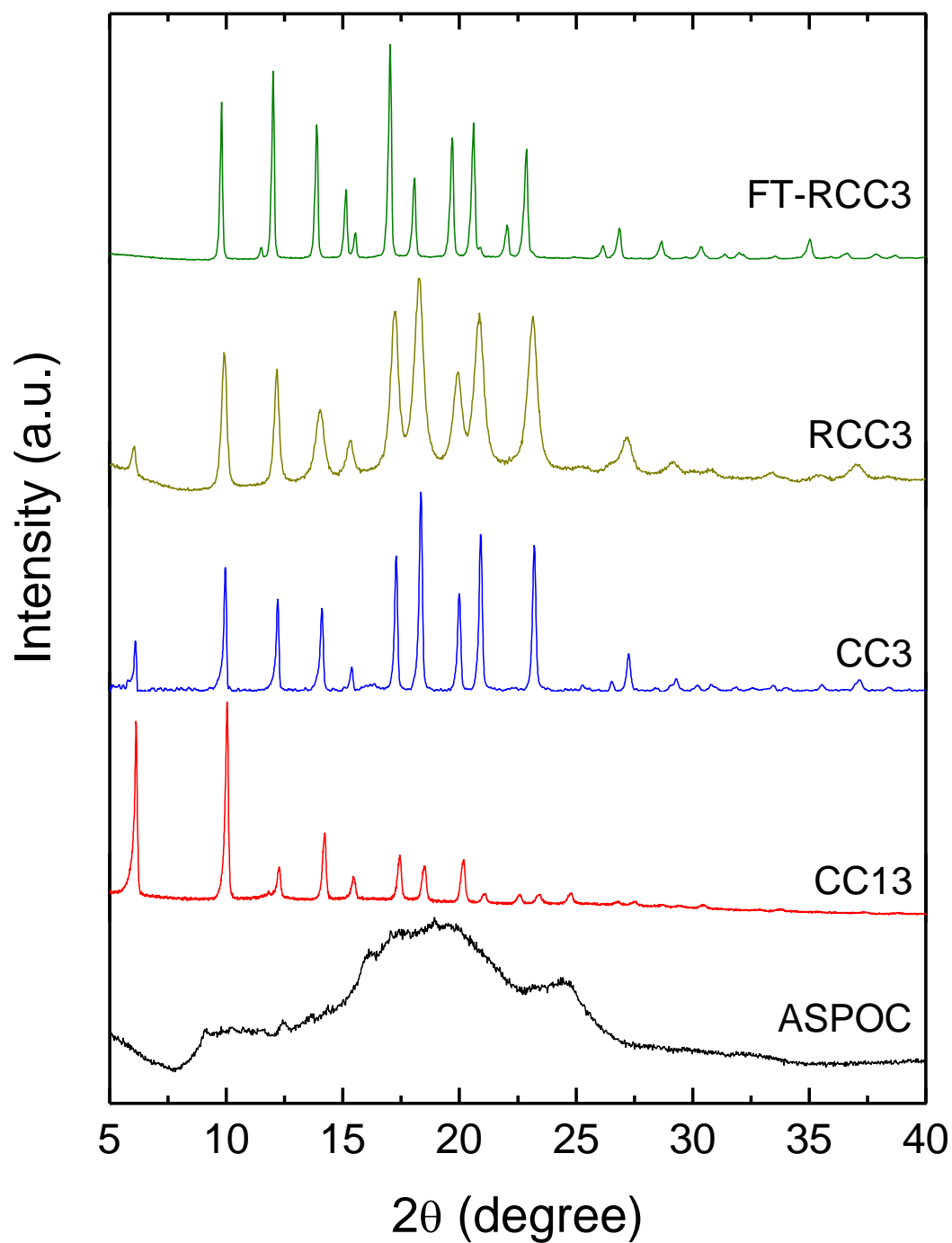


Figure S3. PXRD patterns of porous organic cage powders.

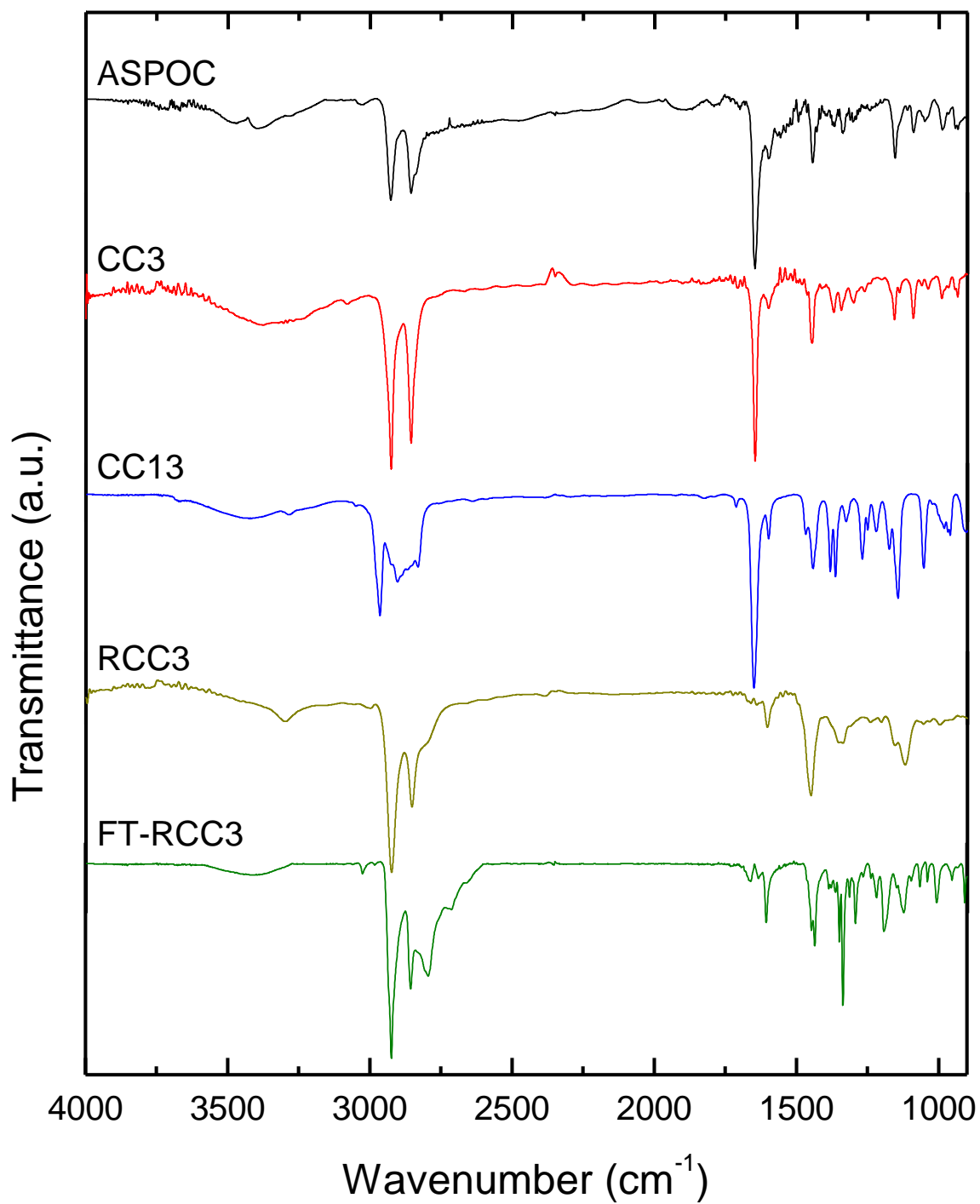


Figure S4. FTIR spectra of POC cages coated on CaCl₂ plates.

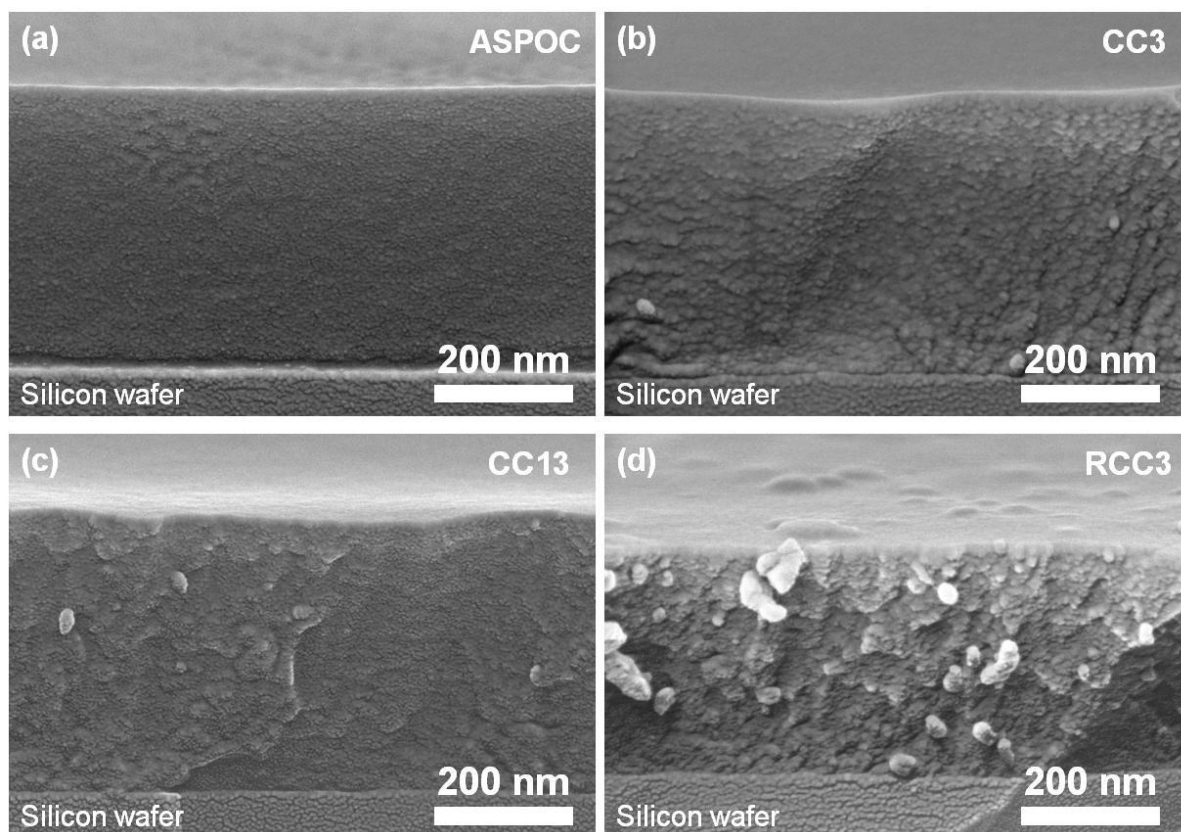


Figure S5. Cross-sectional SEM images of POC thin films coated on silicon wafer substrates. (a) **ASPOC**, (b) **CC3**, (c) **CC13**, and (d) **RCC3**. Cage concentration: (a) 4 wt% in chlorform, (b) 4 wt% in a co-solvent MeOH (2wt%)/DCM (98wt%), i.e. 20 mg **CC3** dissolved in a mixture of MeOH (10 mg) and DCM (490 mg); (c) 4 wt% in chlorform; (d) 4 wt% in chloroform. Spin-coating conditions: 2000 rpm for 60 s, acceleration speed 1500 rpm.

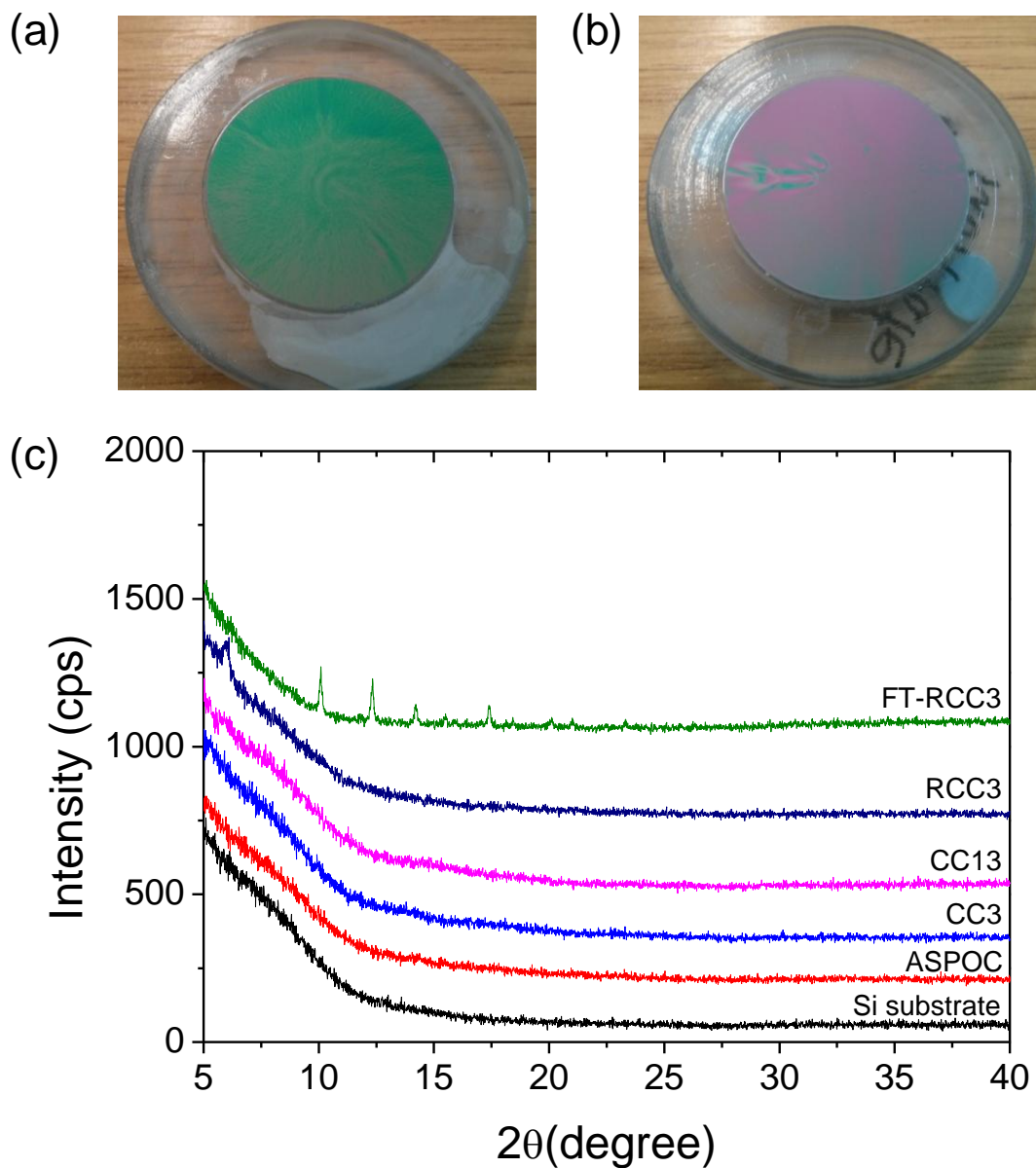


Figure S6. Photographs and XRD patterns of POC thin films coated on low background silicon sample holder. (a) ASPOC, (b) CC3, (c) XRD patterns of POC thin films.

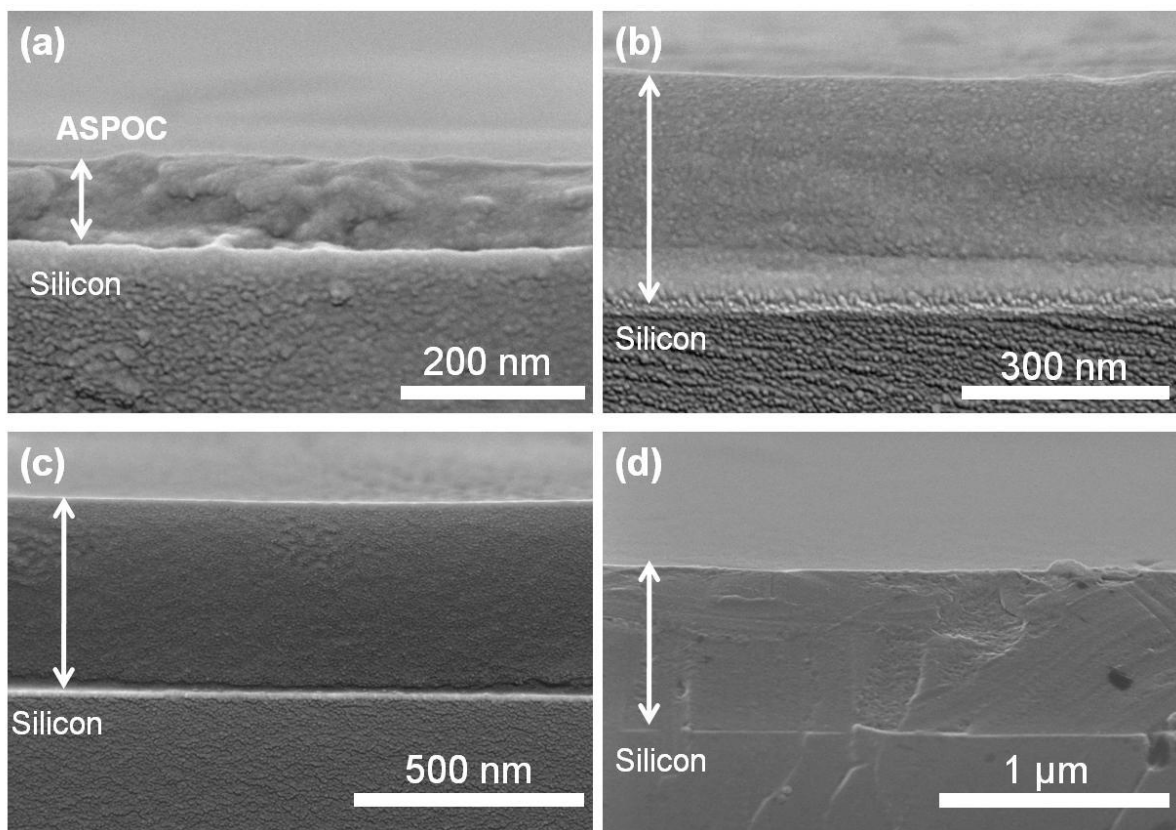


Figure S7. Cross-sectional SEM images of amorphous porous organic cages (ASPOC) coated on silicon wafer with varied thickness. The thickness was tuned by varying the concentration of cage solution in chloroform. (a) 1 wt%, (b) 2 wt%, (c) 4 wt%, (d) 5 wt%.

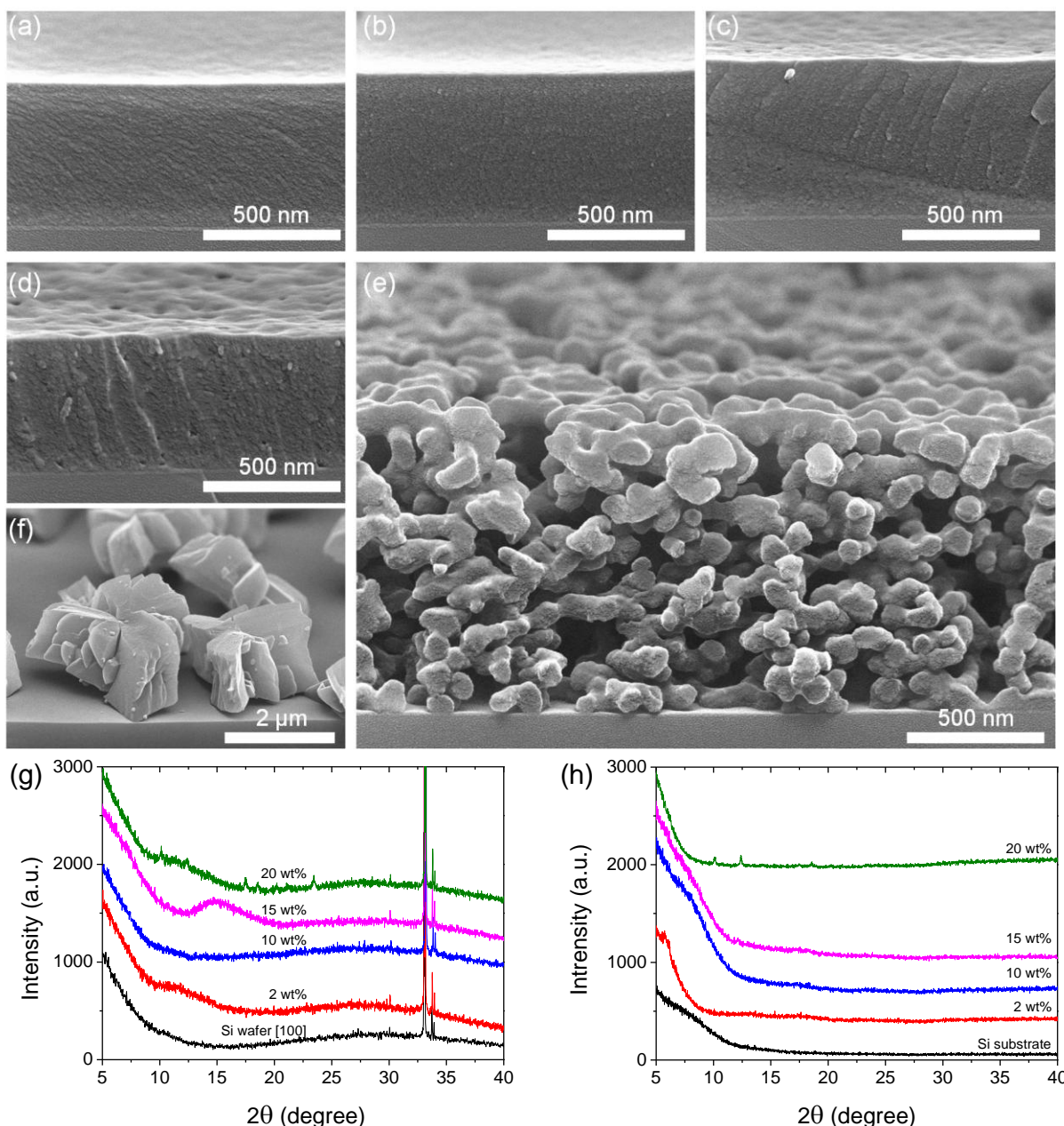


Figure S8. Influence of co-solvent on morphology and crystalline structure of **CC3** cages coated on silicon substrates. The **CC3** cage molecules (4 wt% in solvent) were dissolved in a mixture of dichloromethane (DCM) and methanol, with the weight percentage of methanol in the mixture at (a) 2 wt%, (b) 4 wt%, (c) 6 wt%, (d) 10 wt%, (e) 15 wt%, and (f) 20 wt%. (g) XRD pattern of **CC3** cages coated on silicon wafer [100]. The peaks shown 33-35° correspond to the silicon wafer. (h) PXRD patterns of **CC3** cages coated on low background silicon sample holder. The spin coating was performed at a speed of 2000 rpm for 60 second, with an acceleration speed of 1500 rpm. These thin films are amorphous.

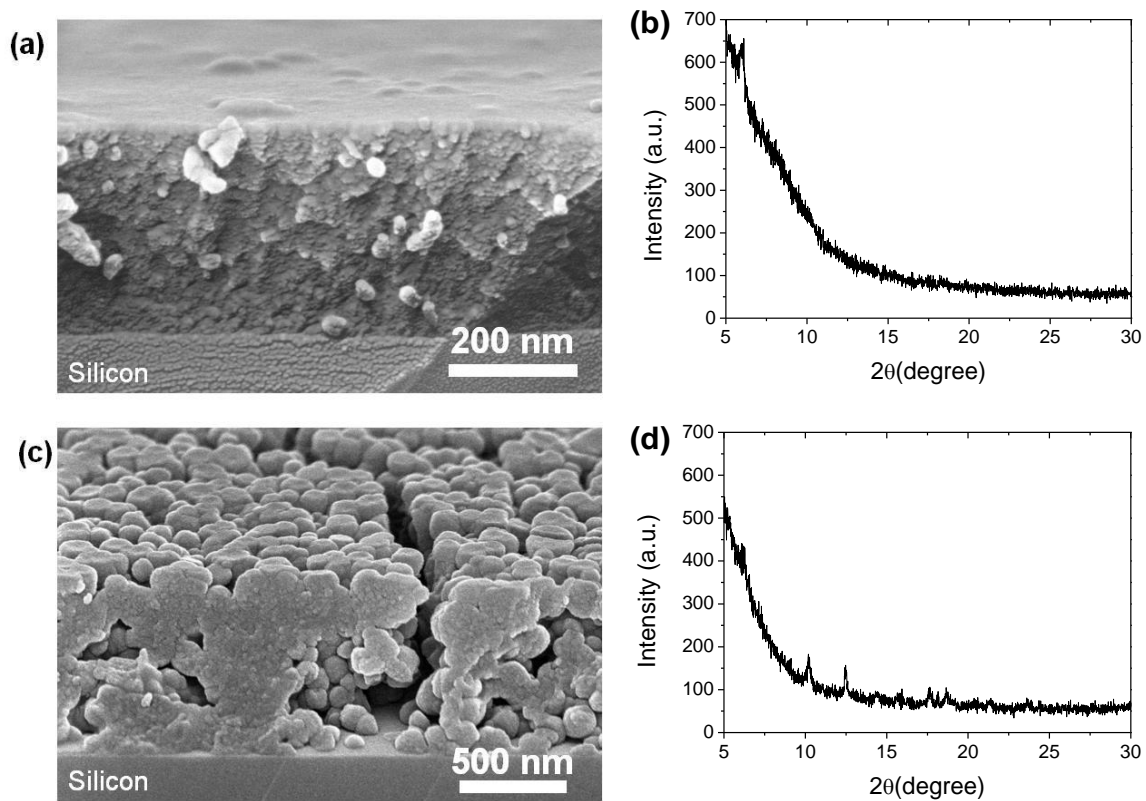


Figure S9. Cross-sectional morphology and XRD patterns of **RCC3** thin films spin-coated at different spinning speeds. (a-b) Spinning speed of 2000 rpm for 60 s, at an acceleration speed of 1500 rpm. (c-d) Spinning speed of 1000 rpm for 60 s, at an acceleration speed of 1500 rpm. The concentration of **RCC3** in chloroform is 4 wt%.

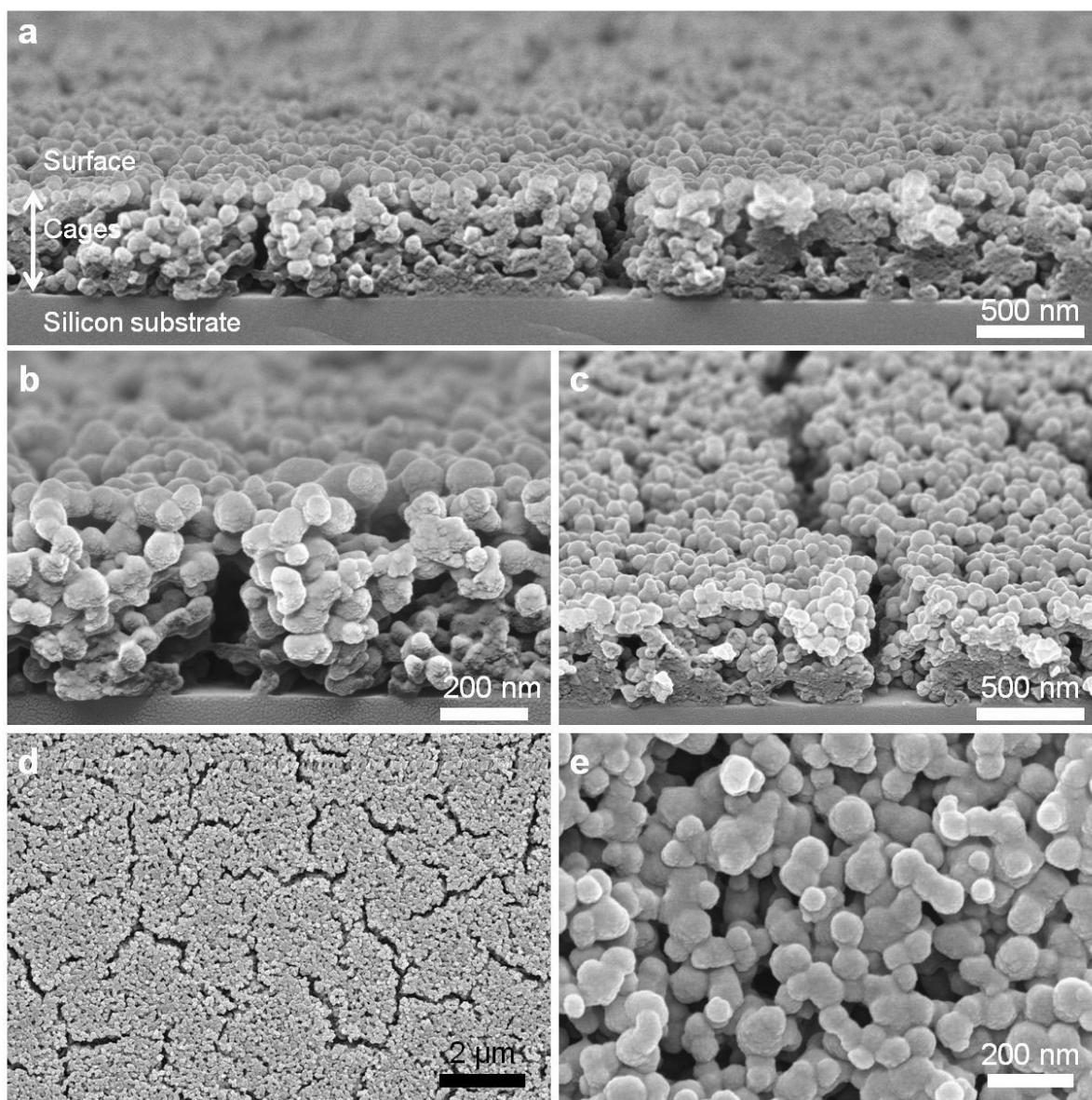


Figure S10. SEM images of hierachically porous thin films of **FT-RCC3** cages coated on silicon substrate. (a-c) Cross-sections and (d-e) surface at different magnifications. Cages (4 wt%) were dissolved in a co-solvent of MeOH (2 wt%)/DCM (98 wt%). Spin-coating condition: 2000 rpm for 60 s, at an acceleration speed of 1500 rpm.

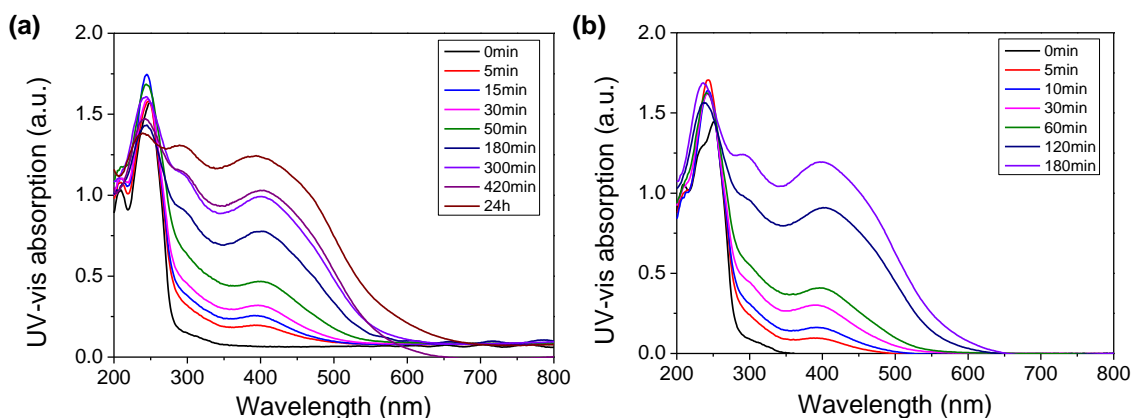


Figure S11. UV-visible absorption spectra of cage thin film (~100 nm) upon exposure to sorption of iodine molecules. (a) **CC3**, (b) **ASPOC**. Note that these experiments were operated manually and *ex situ*, therefore the kinetics of sorption was not strictly controlled. The iodine sorption was also affected by structural change owing to UV-induced photochemical reactions. A control experiment without exposure to UV irradiation confirmed that iodine adsorption and desorption in cage films are reversible.

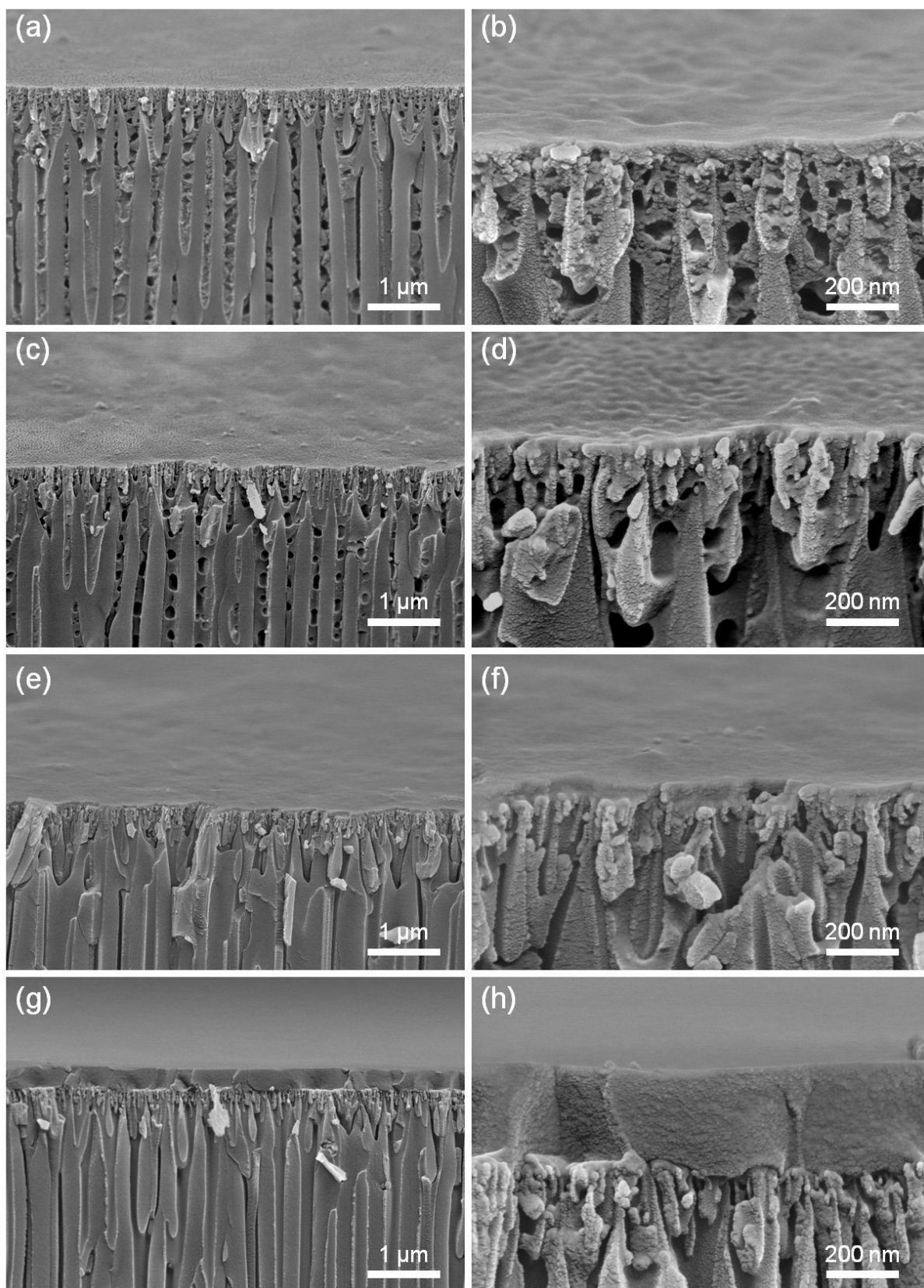


Figure S12. Cross-sectional SEM images of POC thin film composite membranes supported on mesoporous AAO substrates. (a-b) ASPOC, (c-d) CC13, (e-f) CC3 (thickness of 50 nm), (g-h) CC3 (thickness of 300 nm).

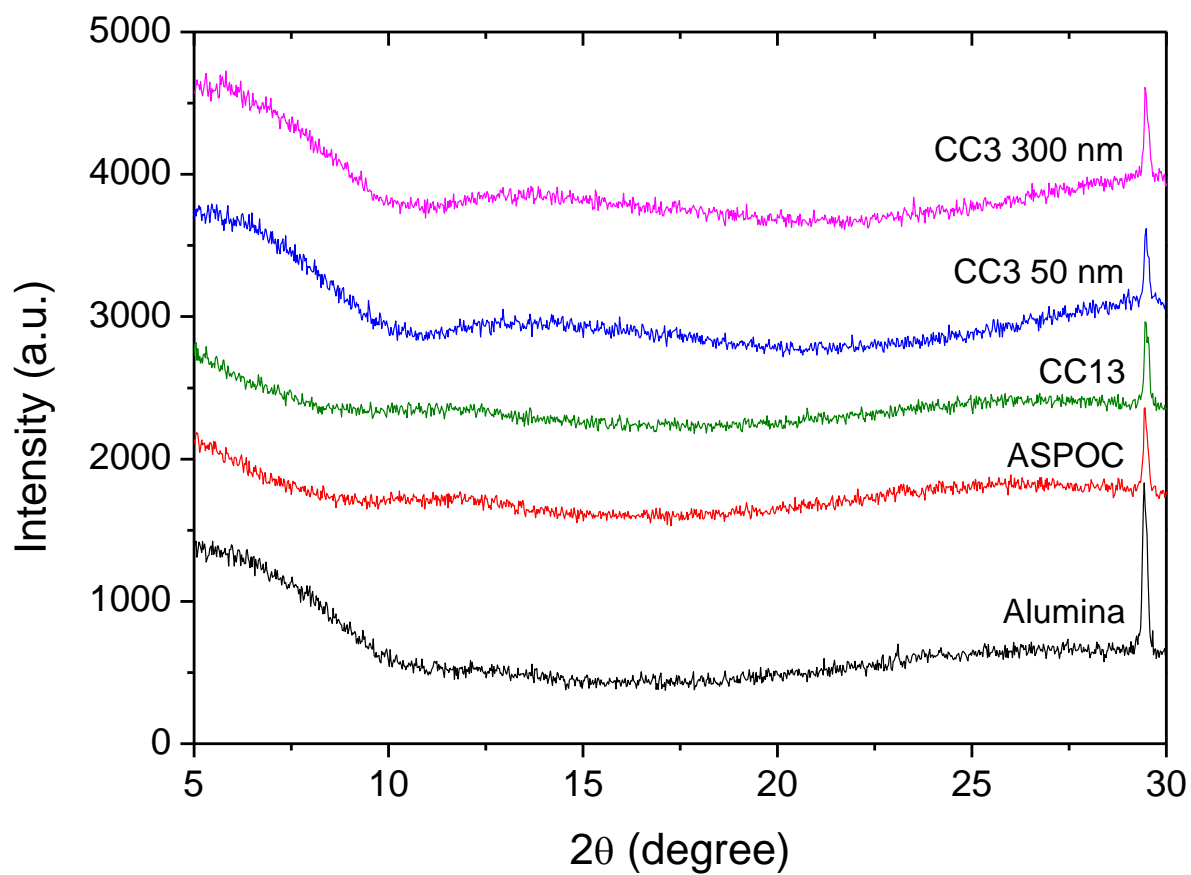


Figure S13. XRD pattern of POC thin films coated on porous alumina support. The peaks at 29° correspond to the alumina support.

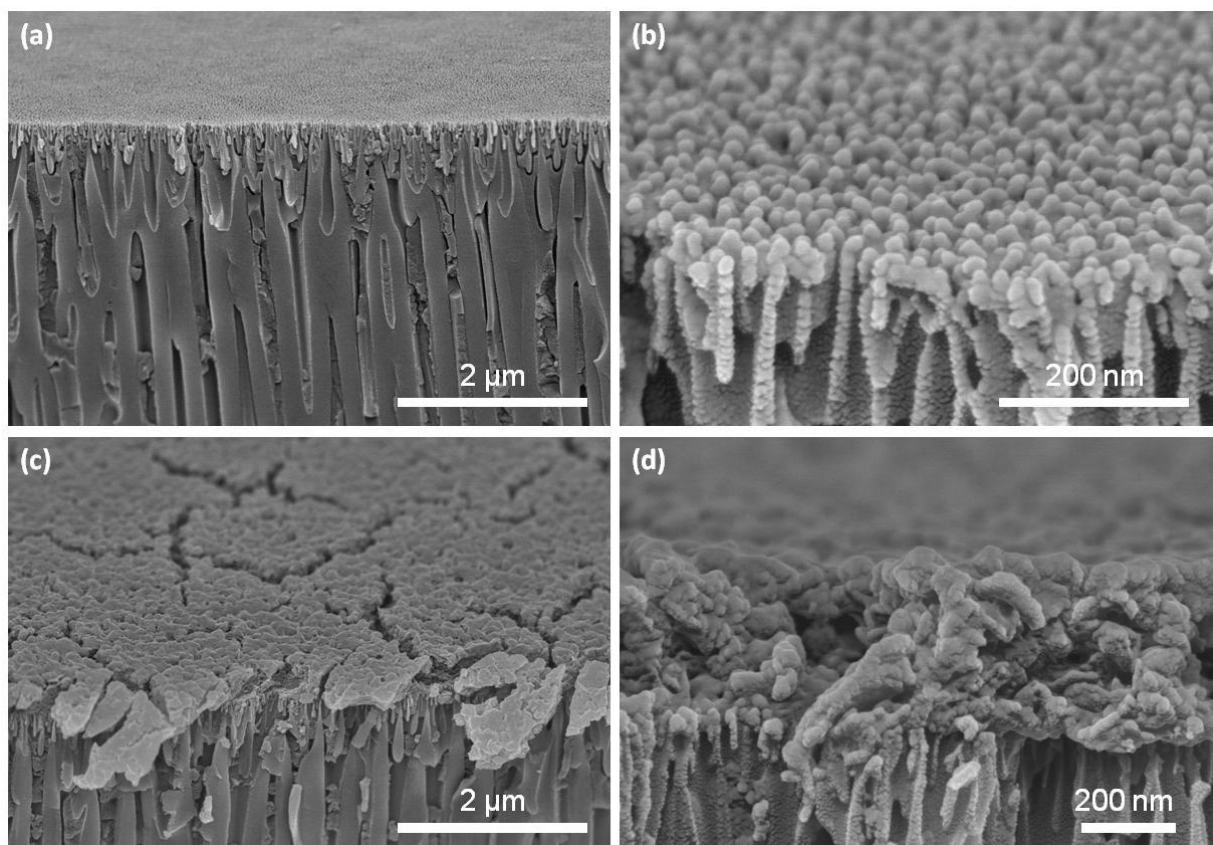


Figure S14. Thin film composite membranes. (a-b) **RCC3**, (c-d) **FT-RCC3**. **RCC3** was dissolved in chloroform (4 wt%). **FT-RCC3** (4 wt%) was dissolved in a co-solvent of MeOH (2wt%)/DCM (98 wt%). Spin-coating condition: 2000 rpm for 60 s, at an acceleration speed of 1500 rpm.

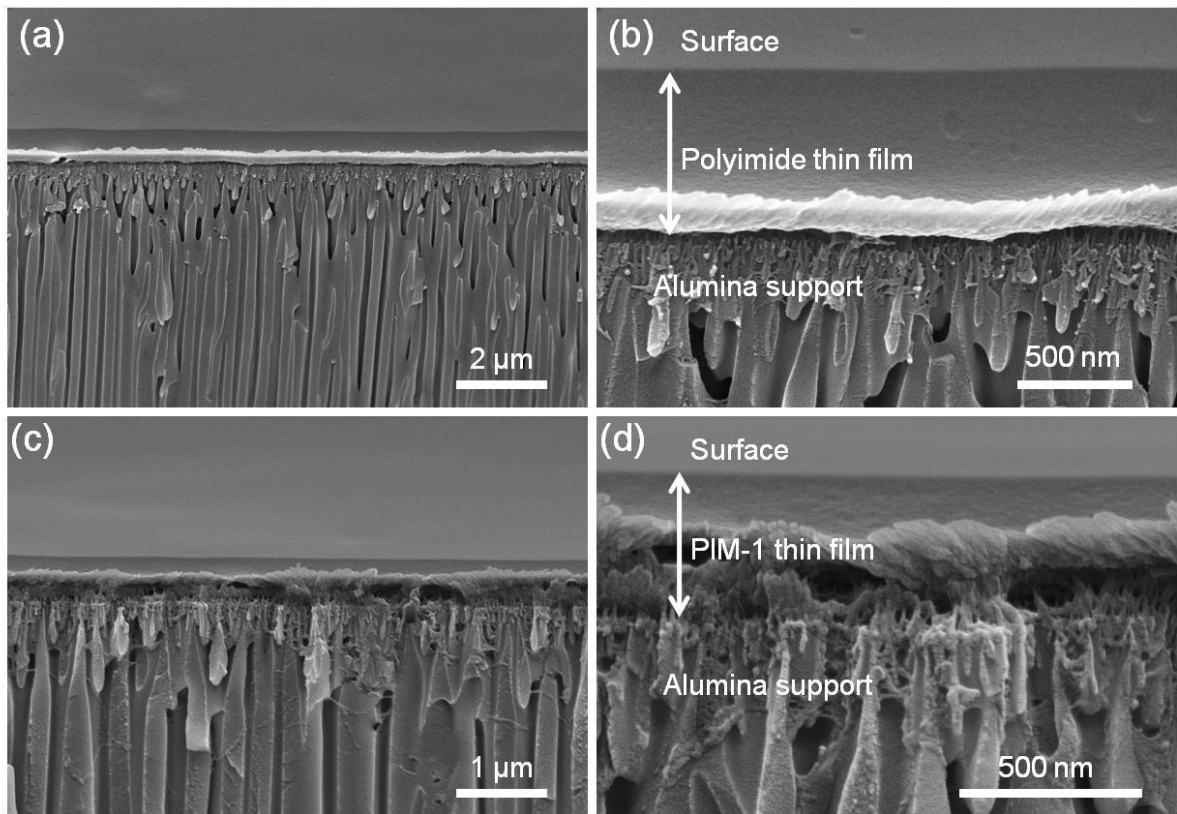


Figure S15. Polymer thin film composite membranes. (a-b) Polyimide Matrimid[®] 5218 spin-coated on porous AAO support. (c-d) PIM-1 polymer spin-coated on porous alumina support.

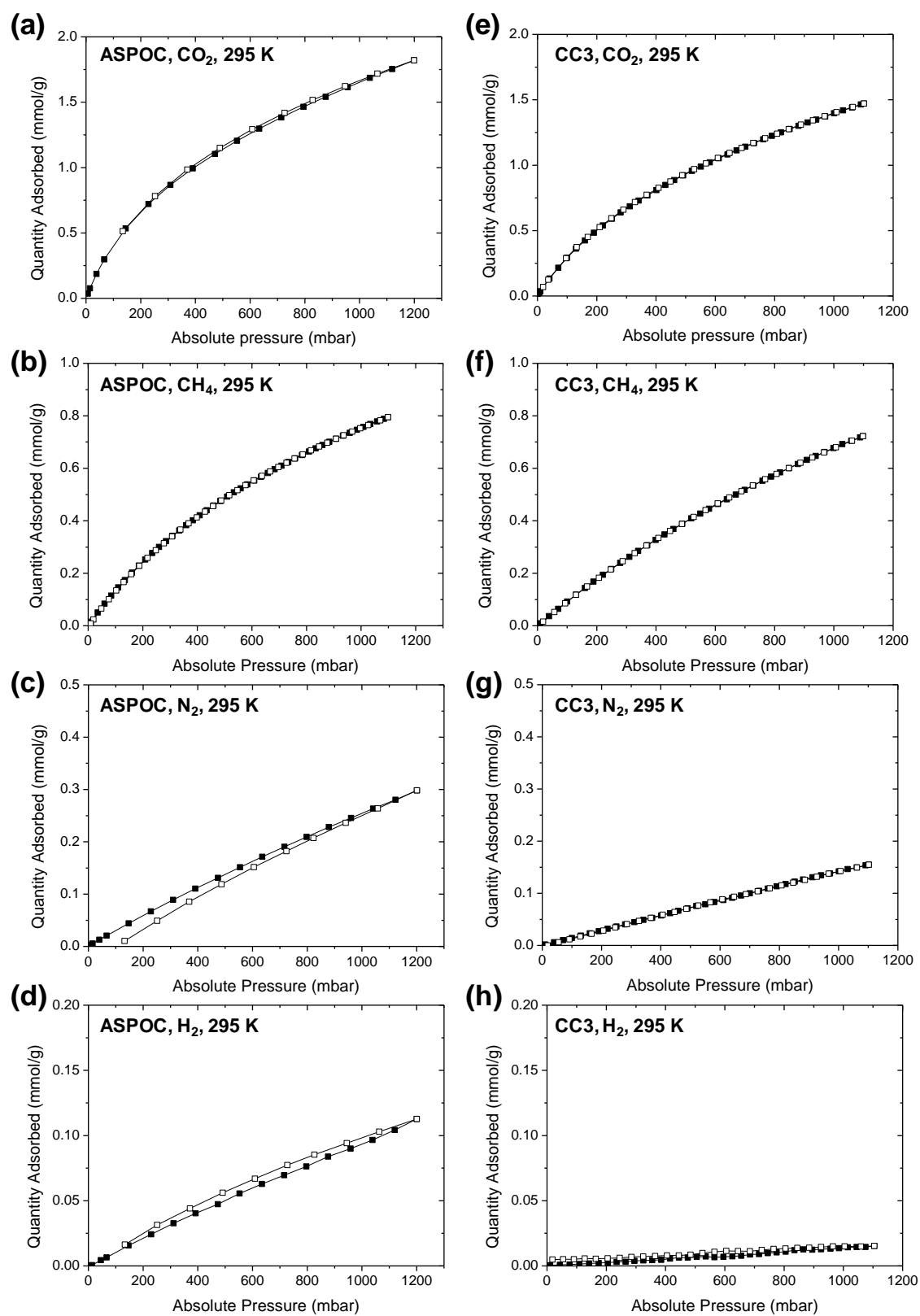


Figure S16. Gas sorption isotherms of ASPOC (a-d) and amorphous CC3 solids (e-h). Amorphous CC3 was prepared by freeze-drying method.

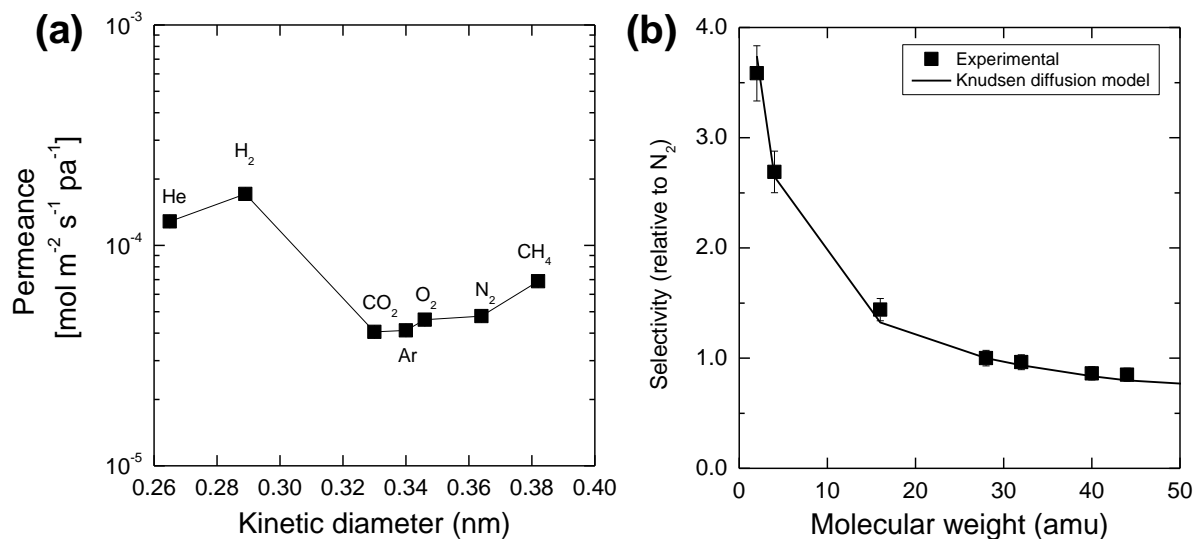


Figure S17. Gas transport properties of porous anodized aluminum oxide (AAO) membrane support (Anodisc, Whatman) with a surface layer of nanopores with pore diameter of 20 nm. (a) Permeances *versus* kinetic diameter of gas molecules, measured at feed pressure of 1 bar and 295 K. (b) Gas permselectivity *versus* the molecular weight. Selectivity is defined as the permeances of H₂, He, CH₄, N₂, O₂, Ar, and CO₂, normalized by N₂ permeance. The selectivity predicted based on Knudsen diffusion model is also included.

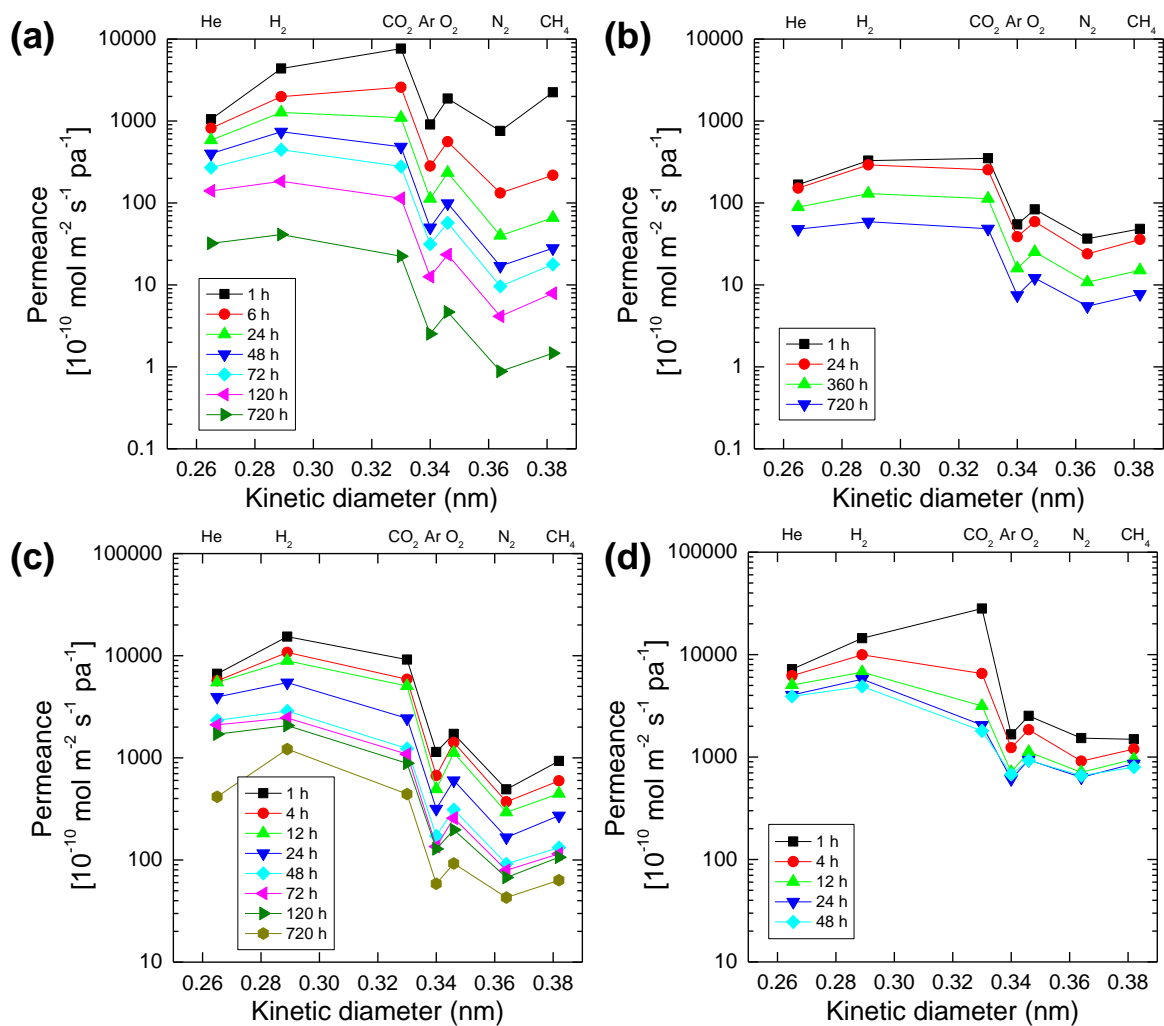


Figure S18. Permeance *versus* kinetic diameter for POC thin film composite membranes exposed to continuous vacuum. (a) ASPOC, (b) CC13, (c) CC3 (thickness of 50 nm), (d) CC3 (thickness of 300 nm).

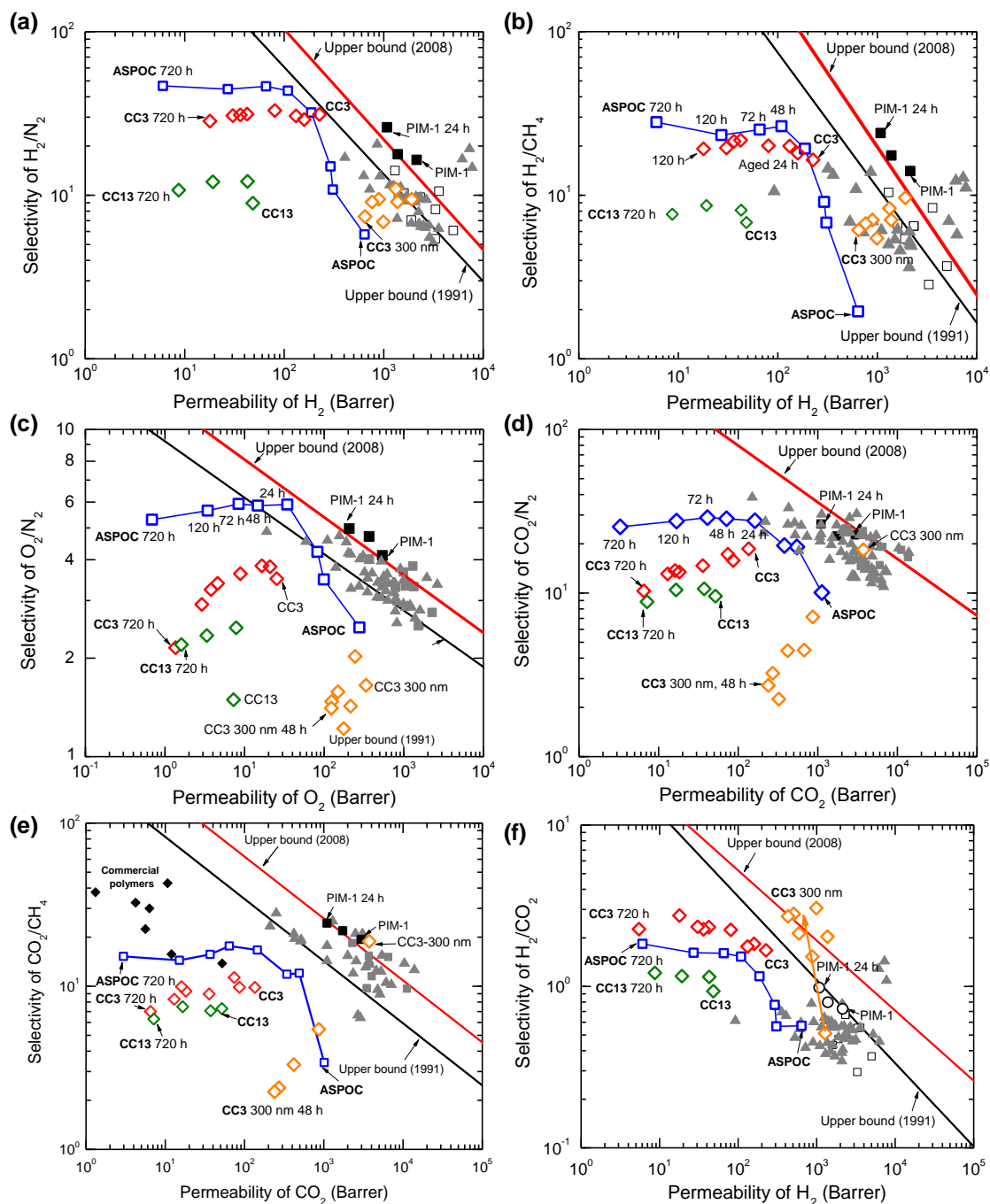


Figure S19. Robeson upper bound plots of selectivity versus permeability for POC thin film composite (TFC) membranes. A representative polymer of intrinsic microporosity (PIM-1), is included for comparison. Triangles: PIMs in the literature.^[2] Upper bound plots are reported by Robeson in 1991 and 2008.^[3]

Table S1. Gas transport properties of porous organic cage thin film membranes. MOF and zeolite membranes are included for comparison.

Materials	Thickness [μm]	Permeance (10^{-8}) [$\text{mol m}^{-2} \text{s}^{-1} \text{Pa}^{-1}$]					Ideal Selectivity					Ref
		H ₂	CO ₂	O ₂	N ₂	CH ₄	CO ₂ /N ₂	CO ₂ /CH ₄	O ₂ /N ₂	H ₂ /N ₂	H ₂ /CH ₄	
Knudsen diffusion							0.8	0.60	0.93	3.7	2.8	[4]
Matrimid	~0.6	1.05	0.698	0.119	0.019	0.017	36.1	41.0	6.2	54.7	62.2	This
PIM-1	~0.45	162.0	223.2	40.6	9.86	11.5	22.6	19.3	4.1	16.4	14.0	This
PIM-1 24h	~0.45	81.6	82.9	15.6	3.14	3.40	26.4	24.4	5.0	26.0	24.0	This
ASPOC	~0.5	43.6	76.4	18.8	75.8	22.4	10.1	3.4	2.5	5.8	1.9	This
ASPOC-24h	~0.5	12.7	10.99	2.34	0.40	0.66	27.7	16.7	5.9	32.0	19.3	This
CC13	~0.5	3.28	3.51	0.84	0.37	0.48	9.6	7.3	1.5	8.9	6.8	This
CC13-24h	~0.5	2.91	2.54	0.59	0.24	0.36	10.6	7.1	2.5	12.2	8.1	This
CC3	~0.3	144.3	281.4	25.3	15.3	14.9	18.4	18.9	1.65	9.4	9.7	This
CC3-24h	~0.3	57.6	20.5	9.35	6.34	8.60	3.2	2.38	1.47	9.1	6.7	This
CC3	~0.05	153.4	91.7	17.2	4.91	9.32	18.7	9.83	3.5	31.2	16.5	This
CC3-24h	~0.05	54.7	24.4	6.01	1.66	2.72	14.7	8.96	3.6	33.0	20.1	This
MOF membranes												
ZIF-7	~1.5	7.4	1.1	-	1.1	1.18	1.0	0.9	-	6.8	6.2	[5]
ZIF-7	~2	4.55	0.35	-	0.22	0.31	1.6	1.1	-	20.9	14.3	[6]
ZIF-8	~30	6.04	1.33	1.04	0.52	0.48	2.6	2.8	2.0	11.6	12.6	[7]
ZIF-8	~20	17.3	4.45	5.22	1.49	1.33	3.0	3.3	3.5	11.6	13.0	[8]
ZIF-8	~20	8.23	-	1.27	0.69	0.63	-	-	1.8	11.9	13.1	[9]
ZIF-22	~40	20.2	2.38	2.80	2.84	3.02	0.8	0.8	1.0	7.1	6.7	[10]
ZIF-22 ^(a)	~40	(~18.0)	2.30	2.95	2.93	3.31	0.8	0.7	1.0	6.4	5.2	[10]
ZIF-90	~20	25.0	3.48	-	1.98	1.57	1.8	2.2	-	12.6	15.9	[11]
ZIF-90 ^(a)	~20	(~24.0)	3.25	-	2.12	1.64	1.5	2.0	-	11.3	15.3	[11]
ZIF-90	~20	21.0	1.34	-	1.28	1.08	1.0	1.2	-	16.4	19.4	[12]
ZIF-90 ^(a)	~20	(~20.0)	1.32	-	1.35	1.03	1.0	1.3	-	14.8	19.4	[12]
HKUST-1	60	100								7	6	[13]
Zeolite membranes												
Zeolite NaX		87.6	17.8		21.3					4.1		[14]
Zeolite P/NaX		13.6	1.65		2.4					5.7		[14]
Silicate-1 MFI	2	790	430		460	640	0.9	0.7		1.7	1.2	[15]
SAPO-34		3.2	2.4		0.43	0.13	5.6	18.5		7.4	24.6	[16]
LTA AlPO ₄	10-20	26.3	2.38	2.92		3.38		0.7			7.8	[17]

Supplementary References

- [1] M. Liu, M. A. Little, K. E. Jelfs, J. T. A. Jones, M. Schmidtman, S. Y. Chong, T. Hasell, A. I. Cooper, *J. Am. Chem. Soc.* **2014**, *136*, 7583-7586.
- [2] a)N. Du, H. B. Park, M. M. Dal-Cin, M. D. Guiver, *Energy Environ. Sci.* **2012**, *5*, 7306-7322; b)C. G. Bezzu, M. Carta, A. Tonkins, J. C. Jansen, P. Bernardo, F. Bazzarelli, N. B. McKeown, *Adv. Mater.* **2012**, *24*, 5930-5933; c)M. Carta, M. Croad, R. Malpass-Evans, J. C. Jansen, P. Bernardo, G. Clarizia, K. Friess, M. Lanč, N. B. McKeown, *Adv. Mater.* **2014**, *26*, 3526-3531; d)B. S. Ghanem, R. Swaidan, E. Litwiller, I. Pinnau, *Adv. Mater.* **2014**, *26*, 3688-3692; e)B. S. Ghanem, N. B. McKeown, P. M. Budd, J. D. Selbie, D. Fritsch, *Adv. Mater.* **2008**, *20*, 2766-2771.
- [3] a)L. M. Robeson, *Journal of Membrane Science* **1991**, *62*, 165-185; b)L. M. Robeson, *J. Membr. Sci.* **2008**, *320*, 390-400.
- [4] R. W. Baker, *Membrane Technology and Applications*, John Wiley & Sons, Ltd, **2004**.
- [5] Y. S. Li, F. Y. Liang, H. Bux, A. Feldhoff, W. S. Yang, J. Caro, *Angew. Chem., Int. Ed.* **2010**, *49*, 548-551.
- [6] Y. Li, F. Liang, H. Bux, W. Yang, J. Caro, *J. Membr. Sci.* **2010**, *354*, 48-54.
- [7] H. Bux, F. Liang, Y. Li, J. Cravillon, M. Wiebcke, J. Caro, *J. Am. Chem. Soc.* **2009**, *131*, 16000-16001.
- [8] M. C. McCarthy, V. Varela-Guerrero, G. V. Barnett, H. K. Jeong, *Langmuir* **2010**, *26*, 14636-14641.
- [9] H. Bux, A. Feldhoff, J. Cravillon, M. Wiebcke, Y. S. Li, J. Caro, *Chem. Mater.* **2011**, *23*, 2262-2269.
- [10] A. Huang, H. Bux, F. Steinbach, J. Caro, *Angew. Chem., Int. Ed.* **2010**, *49*, 4958-4961.
- [11] A. Huang, W. Dou, J. Caro, *J. Am. Chem. Soc.* **2010**, *132*, 15562-15564.
- [12] A. Huang, J. Caro, *Angew. Chem., Int. Ed.* **2011**, *50*, 4979-4982.
- [13] H. Guo, G. Zhu, I. J. Hewitt, S. Qiu, *J. Am. Chem. Soc.* **2009**, *131*, 1646-1647.
- [14] X. Yin, G. Zhu, Z. Wang, N. Yue, S. Qiu, *Microporous Mesoporous Mater.* **2007**, *105*, 156-162.
- [15] C. Algieri, P. Bernardo, G. Golemme, G. Barbieri, E. Drioli, *J. Membr. Sci.* **2003**, *222*, 181-190.
- [16] J. C. Poshusta, V. A. Tuan, J. L. Falconer, R. D. Noble, *Ind. Eng. Chem. Res.* **1998**, *37*, 3924-3929.
- [17] A. Huang, F. Liang, F. Steinbach, T. M. Gesing, J. Caro, *J. Am. Chem. Soc.* **2010**, *132*, 2140-2141.